An oncolytic vaccinia virus encoding hyaluronidase reshapes the extracellular matrix to enhance cancer chemotherapy and immunotherapy

Shibing Wang,[1,2] Yuxin Li,[1] Chuning Xu,[1] Jie Dong,[1] Jiwu Wei [1]

¹State Key Laboratory of Pharmaceutical Biotechnology and Jiangsu Key Laboratory of Molecular Medicine, Medical School of Nanjing University, Nanjing, Jiangsu, China
²Cancer Center, Department of Pathology, Zhejiang Provincial People's Hospital, Affiliated People's Hospital, Hangzhou Medical College, Hangzhou, Zhejiang, China

Correspondence to
Professor Jiwu Wei;
wjw@nju.edu.cn

ABSTRACT

Background The redundant extracellular matrix (ECM) within tumor microenvironment (TME) such as hyaluronic acid (HA) often impairs intratumoral dissemination of antitumor drugs. Oncolytic viruses (OVs) are being studied extensively for cancer therapy either alone or in conjunction with chemotherapy and immunotherapy. Here, we designed a novel recombinant vaccinia virus encoding a soluble version of hyaluronidase Hyal1 (OVV-Hyal1) to degrade the HA and investigated its antitumor effects in combination with chemo drugs, polypeptide, immune cells, and antibodies.

Methods We constructed a recombinant oncolytic vaccinia virus encoding the hyaluronidase, and investigated its function in remodeling the ECM of the TME, the antitumor efficacy both in vitro and in several murine solid tumors either alone, or in combination with chemo drugs including doxorubicin and gemcitabine, with polypeptide liraglutide, with immune therapeutics such as PD-L1/PD-1 blockade, CD47 antibody, and with CAR-T cells.

Results Compared with control OVV, intratumoral injection of OVV-Hyal1 showed superior antitumor efficacies in a series of mouse subcutaneous tumor models. Moreover, HA degradation by OVV-Hyal1 resulted in increased intratumoral dissemination of chemo drugs, infiltration of T cells, NK cells, macrophages, and activation of CD8⁺ T cells. When OVV-Hyal1 was combined with some antitumor therapeutics, for example, doxorubicin, gemcitabine, liraglutide, anti-PD-1, anti-CD47 blockade, or CAR-T cells, more profound therapeutic outcomes were obtained.

Conclusions OVV-Hyal1 effectively degrades HA to reshape the TME, therefore overcoming some major hurdles in current cancer therapy, such as limited OVs spread, unfavored dissemination of chemo drugs, polypeptides, antibodies, and insufficient infiltration of effector immune cells. OVV-Hyal1 holds the promise to improve the antitumor outcomes of current cancer therapeutics.

BACKGROUND

Human solid tumors often establish a number of obstacles to limit chemotherapy and immunotherapy. The primary physical barrier for treatment drugs is the presence of abundant extracellular matrix (ECM) and

WHAT IS ALREADY KNOWN ON THIS TOPIC

⇒ The redundant extracellular matrix (ECM) within solid tumor microenvironment (TME) often limits intratumoral diffusion of antitumor drugs or hinders infiltration of immune cells, which results in poor antitumor efficacy of chemotherapy and immunotherapy.

WHAT THIS STUDY ADDS

⇒ Our present study engineered a novel recombinant oncolytic vaccinia virus encoding the hyaluronidase (OVV-Hyal1) to reshape TME by degrading hyaluronic acid, a major component of ECM of many solid tumors. Intratumoral administration of OVV-Hyal1 facilitated virus spread, chemo drug dissemination, and leukocytes infiltration with TME, which promises to improve the antitumor outcomes of current cancer therapeutics.

HOW THIS STUDY MIGHT AFFECT RESEARCH, PRACTICE OR POLICY

⇒ This study provides rationale for further exploration of OVV-Hyal1 for clinical trials for solid malignancies. Particularly, given that currently available therapies for advanced pancreatic ductal adenocarcinoma (PDAC) are modestly effective, the clinical effectiveness of OVV-Hyal1 might be best evaluated in patients with advanced PDAC in combination with gemcitabine or immune checkpoint blockers.

high interstitial fluid pressure in the tumor microenvironment (TME).[1]

Proteins like collagen, fibronectin, and laminin, as well as non-proteins like hyaluronan (HA), often referred to as hyaluronic acid or hyaluronate, make up the tumor ECM.[2][3] A significant component of ECM, glycosaminoglycan HA often appears in high molecular weight form (>1000 kDa). By interacting with its appropriate cell surface receptors, CD44 and RHAMM, HA controls the growth and invasion of tumor cells and influences the effectiveness of chemotherapy.[4] HA accumulation is strongly associated with

tumor aggressiveness and poor prognosis, including pancreatic,[5] colorectal,[6] gastric,[7] breast,[8] prostate,[9] and ovarian cancer.[10] Several studies showed that HA accumulation within TME hinder lymphocytes infiltration and therefore limit the antitumor efficacy of immune checkpoint blocker (ICB),[11] CAR-T,[12] TIL[13]; HA degradation-enabled anticancer medicines (such as ICBs,[11 14] chemo drugs,[15] and T cells[16]) to access cancerous cells leading to enhanced antitumor outcome. In addition, it was reported that HA accumulation in the TME prevented viral propagation in the tumor mass.[17 18] Therefore, remodeling of TME by degradation of HA may create a favored environment for a wide range of anticancer medicines in solid tumors.

Oncolytic virotherapy for cancer is a novel approach in which oncolytic viruses (OVs) are genetically modified to preferentially replicate in tumor cells or to improve antitumor immune responses.[19 20] Oncolytic vaccinia virus is one of the most commonly used OVs and has been investigated in different tumor types including breast cancer, pancreatic cancer, colorectal cancer, and so on.

In the current study, we engineer a recombinant oncolytic vaccinia virus to encode a gene of a soluble version of hyaluronidase, an enzyme that degrades HA, and investigate its function in reshaping TME, its antitumor effects either alone or in combination with current antitumor therapeutics in a serial of murine xenografted tumors.

METHODS
Cell lines
The American Type Culture Collection (ATCC; Manassas, USA) provided the cell lines HEK293 (CRL-1573), Hela-S3 (CCL-2.2), 4T1 (CRL-2539), and CT26 (CRL-2638). Panc02 and KPC cell lines were stored in our lab. 4T1^{Hyal1} was constructed by stably transfecting 4T1 cells with a lentivirus carrying the Hyal1 gene. Dulbecco's modified Eagle's medium (DMEM; 11965092, ThermoFisher) supplemented with 10% fetal bovine serum (FBS; 16000044, Gibco) was used to sustain HEK293, Hela-S3, Panc02, KPC, 4T1, and CT26 cells. Hela-S3 cells were kept in suspension in a spinner flask in serum-free medium (H740KJ, Basalmedia, Shanghai, China). All cells were grown in an incubator set at 37°C and 5% CO_2.

Oncolytic vaccinia viruses
The control VV was obtained from our previously described laboratory deposit.[21] GenScript (Nanjing, China) produced the Hyal1 gene fragment, which was then subcloned into the shuttle plasmid pVV-Control to create the recombinant plasmid pVV-Hyal1. In this plasmid, Hyal1 is expressed by a synthetic early/later promoter (pSE/L), whereas enhanced green fluorescent protein (EGFP) and guanine-hypoxanthine phosphoribosyl transferase are expressed by a VV p7.5K early/later promoter. To generate oncolytic vaccinia virus encoding the hyaluronidase (OVV-Hyal1), the shuttle plasmid pVV-Hyal1 was homologously recombined with a western

reserve strain of VV (WR-VV; VR-1354; ATCC). In brief, HEK293 cells were infected for 2 hours with the WR-VV at an MOI of 1 before being transfected with the pVV-Hyal1 using the lipofectamine transfection reagent (A12621, ThermoFisher). The EGFP-positive plaques were chosen and 48 hours later planted in plates containing Hela-S3 cells. A conditional DMEM medium containing 250 g/mL xanthine (A601197, Sangon Biotech, Shanghai, China), 25 g/mL mycophenolic acid (A600640, Sangon), and 15 g/mL hypoxanthine (A500336, Sangon) was used to limit the growth of WR-VV. PCR and DNA sequencing were done after many picking and seeding cycles to demonstrate that the recombinant virus was no longer infected with WR-VV. The purified virus was then grown in 6-well plates, cell culture dishes, and cell culture spinner flasks by Hela-S3 cells. The virus titer was determined using the TCID50 method. The following is the calculating formula: Virus titer=$0.7 \times 10 \times 10^{(1+S (D-0.5))}$, where S is log10 (dilution) and D is the total of the positive EGFP ratios in each dilution.

Cell migration and invasion assay
A wound-healing experiment was used to test the cell migration assay. In 6-well plates, 4T1 and 4T1^{Hyal1} cells were cultivated until they produced completely confluent monolayers. After that, a 100 mm "wound" was formed in the monolayer by scratching it with a sterile pipette tip. The cells were cultured in F-12K medium for 24–48 hours after being replaced. An inverted phase contrast microscope was used to inspect and photograph the wound region. Cell invasion was investigated using a transwell system coated in matrigel (8 m, BD). Upper chambers were seeded with 1×10^5 4T1 or 4T1^{Hyal1} cells suspended in serum-free media, whereas bottom chambers received 10% FBS medium. After 24 hours, cells on the upper surface of the filter were removed with a cotton swab. The membrane was then fixed and dyed with crystal violet. A microscope with a magnification of roughly 100 was used to view and count cells on the membrane's lower surface. Five random fields were chosen at random to represent the number of invasive cells in order to quantify positive cells.

Western blot analysis
Tumor cells were seeded at a density of 5×10^5 cells per well in 6-well plates and infected with OVV-Hyal1 or OVV-Ctrl at an MOI of 1. After 48 hours, the cell lysates were collected, and 10 μL of them were mixed in equal amounts with a 2×loading buffer (P0015, Beyotime, Shanghai, China). After heating the protein samples for 5 min at 100°C, they were put onto a sodium dodecyl-sulfate polyacrylamide gel electrophoresis gel for electrophoresis. Using a semi-dry membrane transfer apparatus, the protein on the PAGE gel was transferred to a polyvinylidene fluoride (PVDF) membrane (K5MA6539B, Merck Millipore) after electrophoresis. Subsequently, the PVDF membrane was subjected to an overnight incubation at 4°C with a mouse anti-Hyal1 antibody (25 179-1-AP,

Proteintech, Wuhan, China) and a mouse anti-GAPDH antibody (60004-1-Ig, Proteintech). Next, the goat anti-mouse IgG (H+L) (A0216, Beyotime) was incubated at room temperature for 1 hour. The protein bands were visible using an upgraded chemiluminescent kit (FD8000, FDbio, Hangzhou, China) following the incubation.

Crystal violet staining

4T1, Panc02, and CT26 cells were seeded in 6-well plates at a density of 5×10^4 cells per well, respectively, and cultured in an incubator at 37°C with 5% CO_2 atmosphere. When the tumor cells reached 70% confluence, OVV-Hyal1 and OVV-Ctrl at MOIs of 0, 0.001, 0.01, 0.1, 1, and 10 were introduced to the wells. The supernatants were removed after 72 hours of incubation, and the 0.2% (w/v) crystal violet solution (C0121, Beyotime) was added to the wells for staining. After 5 min, the staining solution was taken from the wells and washed five times with ddH_2O. A scanner was used to capture the image.

MTT assay

Similar to the crystal violet staining experiment, tumor cells were implanted and infected with OVV-Hyal1 and OVV-Ctrl at MOIs of 0, 0.1, 1, and 10. After 72 hours, supernatants were removed and 150 µL of diluted MTT solution (IM0280, Solarbio; Beijing, China) at a final concentration of 0.5 mg/mL was added to each well. The supernatants were removed after 4 hours of incubation, and the formazan crystals were dissolved in 150 µL of isopropanol. An absorbance microplate reader was used to measure the OD value at 570 nm. The cell viability was determined using the formula below: cell viability $(\%)=(OD_{Treatment}-OD_{Blank})/(OD_{Control}-OD_{Blank})\times100\%$.

Viral replication

Panc02, 4T1, and CT26 cells were seeded in 24-well plates at 1×10^4 cells per well and placed in an incubator at 37°C with a 5% CO_2 atmosphere. When the cells were grown to >90% confluency, OVV-Hyal1, and OVV-Ctrl were added to the wells at an MOI of 0.1. After culturing for 24, 48, 72, and 96 hours, the cells lysed by three freeze-thaw cycles, and centrifuged at 3000×g for 10 min. The supernatants were harvested and the virus titer was determined by a TCID50 method. The fold change was calculated relative to the virus titer at indicated hours.

The replication of viruses within tumors or serum was detected using the TCDI50 assay. Briefly, 48 hours after the last viral injection, the mice were euthanized, tumor samples and serum were harvested. Viral titer was determined by a TCID50 method as previously described.

Animal experiments

BALB/c mice and C57BL/6 mice were purchased from the Model Animal Research Center of Nanjing University (Nanjing, China). For the establishment of subcutaneous tumor models, the Panc02, KPC, 4T1, and CT26 tumor cells were implanted subcutaneously into the right flank of the mice. When the tumor reached approximately 50–100 mm^3, the mice were randomly grouped and intratumorally treated with OVV-Hyal1, OVV-Ctrl, or PBS. Tumor diameters were measured every 2 or 3 days and the tumor volume was calculated by the formula $0.5\times length\times width^2$. When the tumor volume reached 2000 mm^3, mice were euthanized. For the combination therapy with OVV-Hyal1 and doxorubicin (S1208, Selleck) or gemcitabine (S1714, Selleck), subcutaneous Panc02 models were established as previously described. Each mouse was injected intraperitoneally with 2 mg/kg of doxorubicin or 5 mg/kg of gemcitabine, which was initiated from the beginning of viral treatment and continued five times every day. For the combination therapy with OVV-Hyal1 and liraglutide (S8256, Selleck), subcutaneous Panc02 models were established as previously described. Each mouse was intramuscular injected with 300 mg/kg of liraglutide, which was initiated from the beginning of viral treatment and continued 12 times every day. For the combination therapy with OVV-Hyal1 and anti-mouse PD-1 antibody (αPD1, Clone RMP1-14, BE0146, BioXCell), subcutaneous Panc02 and KPC models were established as previously described. Each mouse was injected intraperitoneally with 200 µg of αPD1, which was initiated from the next day of viral treatment and continued five times every 2 days. For the combination therapy with OVV-Hyal1 and anti-mouse CD47 antibody (αCD47, Clone MIAP410, BE0283, BioXCell), subcutaneous 4T1 model was established as previously described. Each mouse was injected intraperitoneally with 100 µg of αCD47, which was initiated 1 day post the first viral injection and continued five times every 2 days. For the combination therapy with OVV-Hyal1 and CD19 CAR-T cells, Panc02/CD19 cells were generated to stably express human CD19 antigen on the surface of Panc02 cell membrane through a lentivirus vector. To prepare CAR-T, T cells were obtained from mouse spleen and were stimulated using Dynabeads CD3/CD28 (ThermoFisher, 111456D), and cultured in T cell medium (X-VIVO 15 medium contained 5%FBS and 100IU/mL interleukin 2 (IL-2) (Peprotech, 200-02). After 24 hours, retrovirus mTRv-GFP-CD19CAR was added with MOI at 50. CAR-T cells were then cultured in T cell medium for 10 days. Panc02/CD19 cells were implanted subcutaneously into the right flank of the mice. When the tumor reached approximately 50–100 mm^3, the mice were randomly grouped and intratumorally treated with OVV-Hyal1, OVV-Ctrl, PBS, or one intravenous injection of 1×10^6 CAR-T cells 1 day after the last viral injection. Tumor diameters were measured every 3 days using a vernier caliper and the tumor volume was calculated by the formula $0.5\times length\times width^2$.

RNA sequencing

Mouse tumor tissue was processed to extract and purify total RNA using TRIzol (Cat# 15596018, Invitrogen, USA) and stored at −80°C. The samples were then analyzed by transcriptome using the Illumina NovaSeq 6000 sequencing platform (Majorbio).

Measurement of cytokines

After previously cured mice rechallenge experiment, the mice were sacrificed after anesthesia to obtain spleens and prepare splenocytes. The cultured Panc02, KPC, 4T1, and CT26 cells were seeded into a 6-well plate at the density of 2×10^5 cells per well, and then 1×10^6 splenocytes were added to make the ratio of splenocytes to tumor cells 5:1. Samples were centrifuged at 600 g for 5 min at RT and the supernatants were collected after 48 hours co-culture. ELISA MAX Standard Sets of interferon-gamma (IFN-γ) (430801, Biolegend), tumor necrosis factor-alpha (TNF-α) (430901, Biolegend) and IL-2 (431001, Biolegend) were used to determine the concentration of the corresponding cytokines. The measurement method was based on the manufacturing protocol.

Flow cytometry

The follows antibodies were purchased from BioLegend: APC anti-CD3 (100236), FITC anti-CD4 (100406), PE anti-CD4 (100408), FITC anti-CD8a (100706), PE anti-CD45 (103106), PE/Dazzle 594 anti-PD-1 (135227), APC/Fire 750 anti-IFN-γ (505860), APC/Fire 750 anti-CD11c (117352), APC anti-CD11b (101212), FITC anti-Ly-6G/Ly-6C (108406), Alexa Fluor 647 anti-LAG-3 (125241), Brilliant Violet 711 anti-Tim-3 (119727), Percp anti-F4/80 (123126), Percp anti-CD86 (105026), FITC anti-CD206 (141704), PE anti-Foxp3 (126404), PE anti-CD44 (103008), FITC anti-CD62L (104406), Percp/Cy5.5 anti-CD152 (106315), Percp/Cy5.5 anti-TNF-α (506322), PE anti-CD47 (506322), APC/Fire 750 anti-CD49a (142609), PE Goat anti-IgG (405307). For the preparation of single-cell suspensions of tumor tissues, mice were anesthetized and sacrificed, and the tumor tissues were harvested and placed in a serum-free medium (H740KJ, Basalmedia) with 0.2% collagenase IV (C4-22-1G, Sigma-Aldrich). Then, the tumor tissues were cut into 1–2 mm pieces, digested for 2 hours, and passed through 70 μm nylon filters (CSS013070, Jetbiofil, China) to obtain the single-cell suspensions. For the preparation of splenocytes, the spleens were obtained from the sacrificed mice and ground into single-cell suspensions using syringe plungers on 70 μm nylon filters. Then, the cells were counted and adjusted to 5×10^6 cells/mL. For tumor cell lines, the adherent cells were digested with 0.5% trypsin in advance. For extracellular staining, the pre-prepared single-cell suspensions were incubated with the fluorescent monoclonal antibodies for 15 min at RT. After incubation, the cells were fixed with 4% (w/v) paraformaldehyde (PFA, Cat# P0099, Beyotime) and subjected to NovoCyte cytometry (Agilent; California, USA). For intracellular staining, the fixed cells were ruptured with 1×permeabilization buffer (Cat# P0099, Beyotime), and then the corresponding antibodies were added followed by another 30 min incubation in the dark. After washing with PBS once, cells were resuspended in PBS and analyzed by flow cytometry. Data analysis was performed using FlowJo software (TreeStar; OR, USA).

Immunohistochemistry

After being treated with 4% PFA, the tumor tissues were embedded in paraffin blocks (G1101, Servicebio). Sections were cut at a thickness of 5 m from paraffin-embedded blocks, deparaffinized in xylene for 10 min, rehydrated in graded ethanol for 10 min, 9 min, 70 min, and 50% min, and then incubated with 3% (w/v) hydrogen peroxide to inhibit endogenous peroxidase activity. The slices were subsequently incubated with a secondary HRP goat anti-rabbit IgG antibody (G1213, Servicebio) and a rabbit anti-CD8 antibody (ab217344, Abcam, USA), a rabbit anti-CD68 antibody (ab283654, Abcam), a rabbit anti-collagen I antibody (ab2709934, Abcam), a rabbit anti-collagen III antibody (ab184993, Abcam), a rabbit anti-elastin antibody (ab307150, Abcam), a rabbit anti-fibronectin antibody (ab268020, Abcam) and a rabbit anti-mouse FMC63 scFv antibody (BIOSWAN, Shanghai, China). Finally, the slices were stained with 3′,3-diaminobenzidine (G1212-2, Servicebio) and counterstained with 37% (w/v) hematoxylin (G1004, Servicebio).

## Terminal deoxynucleotidyl transferase dUTP nick end labeling assay

Tumors were removed, fixed, and embedded in paraffin. Tissue sections were deparaffinized in xylene, rehydrated in graded alcohol, and transferred to PBS. The tissue slices were treated with proteinase K (20 mg/mL) for 15 min, and endogenous peroxidase was blocked using 3% hydrogen peroxide in PBS for 12 min. The One Step TUNEL Cell Apoptosis Detection Kit (Green Fluorescence, Cat# C1086, Beyotime) was used. Terminal deoxynucleotidyl transferase dUTP nick end labeling-positive cells were observed by fluorescence microscopy (Nikon, Japan).

Histological analysis of transplanted tumors

The transplanted Panc02 tumors were isolated 48 hours after last viral injection, and were fixed with 4% paraformaldehyde solution, embedded in paraffin, and cut into 5 μm sections. The tumor collagen components were determined by Masson trichrome staining kit according to the manufacturer's instruction, collagen in tumor spheroids was detected using picrosirius red staining. Collagen fibers and muscle fibers are stained by Van Gieson staining.

Statistical analyses

For all statistical studies, Prism V.8.2.1 (GraphPad Software) was used. The statistical variances between the groups were examined using analysis of variance. The Kaplan-Meier method was used to generate the survival curve, and the log-rank test was used to establish statistical significance across groups. In all statistical studies, $p < 0.05$ was considered statistically significant.
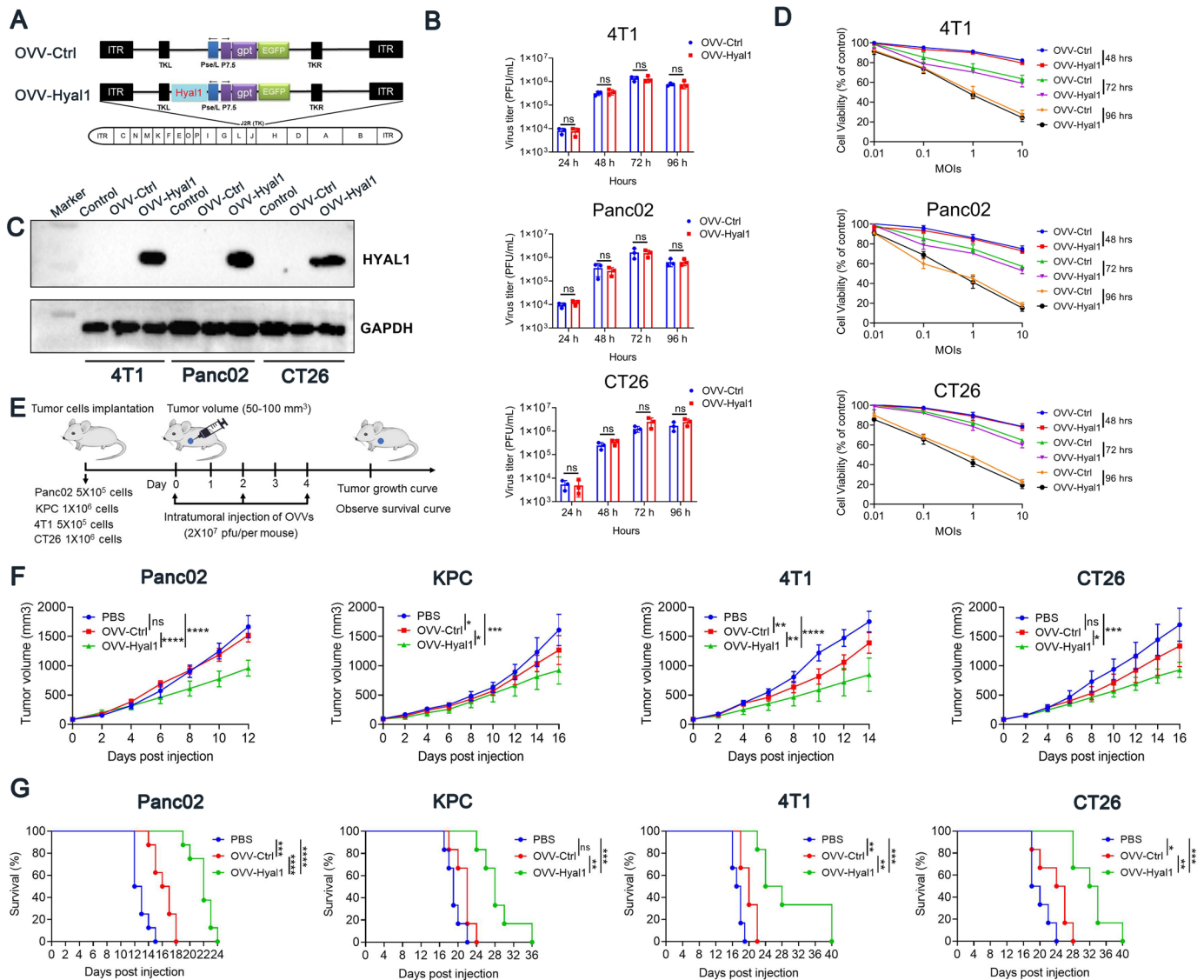
Figure 1 Characterization of oncolytic vaccinia virus encoding the hyaluronidase (OVV-Hyal1) and intratumoral injections of OVV-Hyal1 enhances antitumor efficacy in subcutaneous tumor models. (A) A schematic diagram of homologous recombination. To generate OVV-Hyal1, a shuttle plasmid pVV-Hyal1 was used for homologous recombination with a western reserve (WR) strain of VV by using the left (L) and right (R) flanking sequences of thymidine kinase (TK). (B) TCID50 method was used to detect viral replication in murine tumor cells. (C) Western blot analysis of OVV-Hyal1-induced HYAL1 overexpression in three murine tumor cell lines. (D) MTT assay was used to detect the oncolytic ability of OVV-Hyal1 and OVV-Ctrl against murine tumor cells. (E) 5×10^5 Panc02, 1×10^6 KPC, 5×10^5 4T1, and 1×10^6 CT26 were inoculated into the right flank of C57BL/6 or BALB/c mice. When tumor volume reached approximately 50 to 100 mm^3, mice were administered intratumorally (IT) with either 2×10^7 pfu OVV-Hyal1 or equal dose of OVV-Ctrl every other day for a total three times. Mice received PBS intratumoral injections were used as untreated controls. (F) Tumor volume were measured every two days. Error bars represent SD. Once the tumor volume exceeded 2000 mm^3, the mouse was considered dead. (G) Kaplan-Meier survival analysis of tumor-bearing mice treated with PBS (control), OVV-Ctrl, or OVV-Hyal1. Error bars represent SD. ns, not significant; *p<0.05; **p<0.01; ***p<0.001; ****p<0.0001.

RESULTS

Hyal1-armed oncolytic vaccinia virus improves antitumor activity

In the backbone of a thymidine kinase (TK)-destroyed vaccinia virus WR strain, we inserted a murine Hyal1 gene fragment (OVV-Hyal1) by homologous recombination. The OVV without any other gene insertion in the TK area was generated as control (OVV-Ctrl, figure 1A). The recombinant OVV-Hyal1 could efficiently infect cancer cells and replicate in host cells (figure 1B, online supplemental figure S1), and Hyal1 was massively expressed in a series of cell lines infected with OVV-Hyal1 (figure 1C). In vitro, OVV-Hyal1 exerted a similar oncolysis in malignant cells as OVV-Ctrl (figure 1D).

We further evaluated the antitumor activity of OVV-Hyal1 in several subcutaneous tumor models, including Panc02 and KPC pancreatic carcinoma, 4T1 breast cancer, and CT26 colorectal cancer (figure 1E). In each tumor
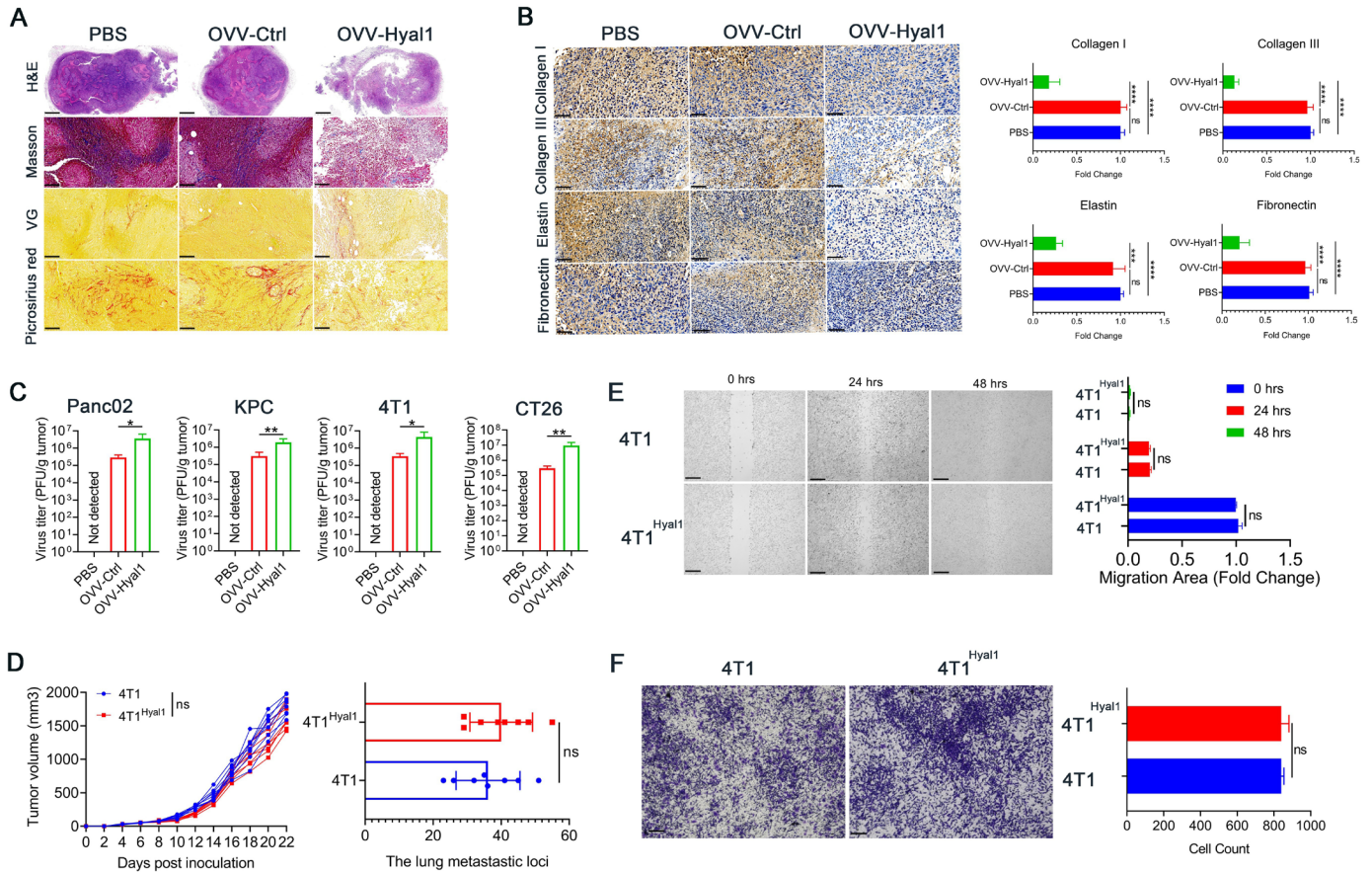
Figure 2 OVV-Hyal1 induces extracellular matrix (ECM) degradation and enhances OVVs replication in vivo. (A, B) 5×10^5 Panc02 injected into the right flank of C57BL/6 mice. When the tumor reached approximately 50–100 mm³, mice were administered intratumorally (IT) with either 2×10^7 pfu OVV-Hyal1 or the equal dose of OVV-Ctrl. Mice received PBS IT was used as untreated control. Tumors were isolated 48 hours after last viral injection and tissue slices were then stained by (A) H&E, Masson, Van Gieson (VG) and picrosirius red staining, and (B) immunohistochemical staining for collagen I, collagen III, elastin, fibronectin. Microscopic images were analyzed semi-quantitatively, and the expression levels of ECM components were expressed as fold change relative to untreated controls. Data are presented as means±SD. Scale bars are equal to 625 µm for H&E and 100 µm for Masson, VG, picrosirius red staining, and immunohistochemistry. (C) The virus titers in tumor tissues or sera of Panc02, KPC, 4T1 and CT26 mice were quantified by the TCID50 method. Error bars represent SD. (D) The subcutaneous tumor models of 4T1^Hyal1 and parental 4T1 were established by inoculation of same number of cells (5×10^5 cells) on the right flank of BALB/c mice. At the end of the mouse experiment, take the mouse lungs and count the number of metastatic lesions. Data are presented as means±SD. (E) Cell scratch assay was used to detect the migration ability of 4T1^Hyal1 cells. Scale bars are equal to 100 µm. (F) Transwell experiment was used to detect the metastation ability of 4T1^Hyal1 cells. Scale bars are equal to 100 µm. Data are presented as means±SD. ns, not significant; *p<0.05; **p<0.01; ***p<0.001; ****p<0.0001.

model, intratumoral injection of OVV-Hyal1 significantly inhibited tumor growth compared with both OVV-Ctrl and PBS treatment (figure 1F, online supplemental figure S2A). Consistently, OVV-Hyal1 treatment significantly prolonged survival compared with OVV-Ctrl and/or PBS (figure 2G). No obvious side effects were observed as monitored by mouse body weight (online supplemental figure S2B).

OVV-Hyal1 effectively degrades ECM components

We further investigated the tumor ECM alteration after intratumoral OVV-Hyal1 injection. Desmoplasia in pancreatic cancer is characterized by collagen-rich tumor and fibrillar collagen (collagen I and collagen III), which speeds up tumor growth and serves as a physical barrier that inhibits drug transport,

producing poor therapeutic results.[22 23] In subcutaneous pancreatic carcinoma Panc02 tumor tissues, we found that OVV-Hyal1 treatment induced a significant decrease of ECM components compared with untreated controls or OVV-Ctrl treatment (figure 2A). We further examined the levels of several major ECM components including collagen I/III, fibronectin, and elastin after OVV-Hyal1 treatment. Intratumoral administration of OVV-Hyal1 resulted in by 82% decrease of collagen I, 87% decrease of collagen III, 73% decrease of elastin fibronectin and 80% decrease of elastin, respectively, compared with OVV-Ctrl treatment (figure 2B).

We then investigated whether ECM degradation by OVV-Hyal1 would improve viral spread in TME.

Indeed, virus titers were significantly increased in OVV-Hyal1-treated tumors than those treated with OVV-Ctrl (figure 2C). Of note, no viruses were detected in the sera from the mice treated with either OVV-Ctrl or OVV-Hyal1 (online supplemental figure S3A).

Moreover, to address the concern whether ECM degradation by HYAL1 would promote metastatic spread of the primary tumor, we generated a murine breast cancer 4T1 cells that constitutively express Hyal1 (4T1[Hyal1], online supplemental figure S3B). Compared with the parental 4T1, 4T1[Hyal1] showed similar growth in mice and comparable lung metastatic nodules (figure 2D), and in vitro migration (figure 2E,F). These data indicate that local expression of Hyal1 did not facilitate malignant cell invasion and metastasis.

Taken together, our data showed that OVV-Hyal1 effectively degraded ECM components leading to enhanced intratumoral viral spread, nevertheless, ECM degradation by Hyal1 did not promote tumor metastasis.

OVV-Hyal1 significantly improves chemotherapy and GLP1-mediated antitumor efficacy

Pancreatic carcinoma is often characterized as an HA-rich "hard" tumor, which displays chemoresistance due to poor drug diffusion within tumor mass. Having shown that OVV-Hyal1 treatment reduced ECM components, we then investigated the antitumor efficacy by combining OVV-Hyal1 with chemotherapeutic agents, such as doxorubicin and gemcitabine (figure 3A). We found that OVV-Hyal1 increased doxorubicin diffusion and enrichment in the tumor (figure 3B), and significantly enhanced the antitumor efficacy of doxorubicin compared with either doxorubicin single treatment or in combination with OVV-Ctrl (figure 3C).

Similarly, OVV-Hyal1 significantly enhanced the antitumor efficacy of gemcitabine compared with either gemcitabine single treatment or in combination with OVV-Ctrl (figure 3D,E), and significantly prolonged lifespan of the mice bearing subcutaneous pancreatic cancer Panc02 xenograft (figure 3F). Of note, two out of eight mice treated with OVV-Hyal1 and gemcitabine obtained tumor complete remission (CR), and three out of eight mice obtained partial remission (PR) (figure 3E). No significant changes in body weight were observed (figure 3G). In line with these findings, OVV—combination of Hyal1 and gemcitabine treatment resulted in marked increase of apoptosis of cancer cells compared with either gemcitabine single treatment or in combination with OVV-Ctrl (figure 3H). However, we noticed that tumor growth progressed in two mice treated with OVV-Hyal1 and gemcitabine. Therefore, we further analyzed the ECM degradation in tumors isolated from mice either obtained PR or progressive disease (PD). The Masson staining showed that ECM was degraded to a higher extent in the PR group than PD group (online supplemental figure S4).

We further investigated if OVV-Hyal1 could also improve polypeptide-mediated antitumor effects. Our previous study showed that GLP1 analog liraglutide possessed the antitumor effect in hepatocellular carcinoma,[24] therefore, we evaluated the antitumor efficacy of OVV-Hyal1 combined with liraglutide in pancreatic carcinoma (figure 3I). We found that OVV-Hyal1 significantly enhances the antitumor efficacy of liraglutide compared with either liraglutide treatment alone or in combination with OVV-Ctrl in a subcutaneous pancreatic carcinoma model (figure 3J,K), two out of eight mice obtained CR (figure 3K). The combined therapy significantly prolonged lifespan of the mice bearing subcutaneous pancreatic cancer Panc02 xenograft (figure 3L). No significant changes in body weight were observed (figure 3M).

Taken together, these results demonstrate that OVV-Hyal1 was able to improve the antitumor outcomes of some chemo drugs as well as polypeptide such as GLP1 analogs in highly desmoplastic pancreatic tumors.

OVV-Hyal1 facilitates lymphocytes infiltration and improves the antitumor efficacy of CAR-T cells in pancreatic cancer

Lymphocytes infiltration is associated with antitumor immune responses. We further investigated if ECM components degradation by OVV-Hyal1 could facilitate the infiltration of immune cells in solid tumors. In pancreatic Panc02 carcinoma model, intratumoral injection of OVV-Hyal1 significantly facilitated leukocytes infiltration in tumor, both T and NK cells were significantly increased in OVV-Hyal1 treated tumors compared with those treated with either OVV-Ctrl or PBS (figure 4A). The increased infiltration of cytotoxic $CD8^+$ T cells was also observed in pancreatic carcinoma tissues by immunohistochemistry (IHC) (online supplemental figure S5). Similar increase of lymphocyte infiltration were also observed in a KPC pancreatic cancer and 4T1 breast cancer (figure 4B,C). Concurrently, the proportion of $CD8^+$ T and $CD4^+$ T cells in the splenocytes were increased after intratumoral injection of OVV-Hyal1 (online supplemental figure S6).

We anticipated that increased lymphocytes infiltration by OVV-Hyal1 would enhance CAR-T cell-mediated antitumor efficacy (figure 4D). To this end, we generated CD19-specific CAR-T cells (CD19-CAR-T), which exerted specific cytotoxicity on Panc02/CD19 cells (Panc02 cells stably expressing the human CD19 antigen) in a dose-dependent manner (online supplemental figure S7). Indeed, intratumoral injection of OVV-Hyal1 significantly improved the therapeutic outcomes of CD19 CAR-T cells compared with either CAR-T cells monotherapy or in combination with OVV-Ctrl (figure 4E,F). 60% (three out of five mice) were cured by OVV-Hyal1 combined with CAR-T cells (figure 4F). Consistently, OVV-Hyal1 combined with CD19 CAR-T significantly prolonged the survival time compared with other
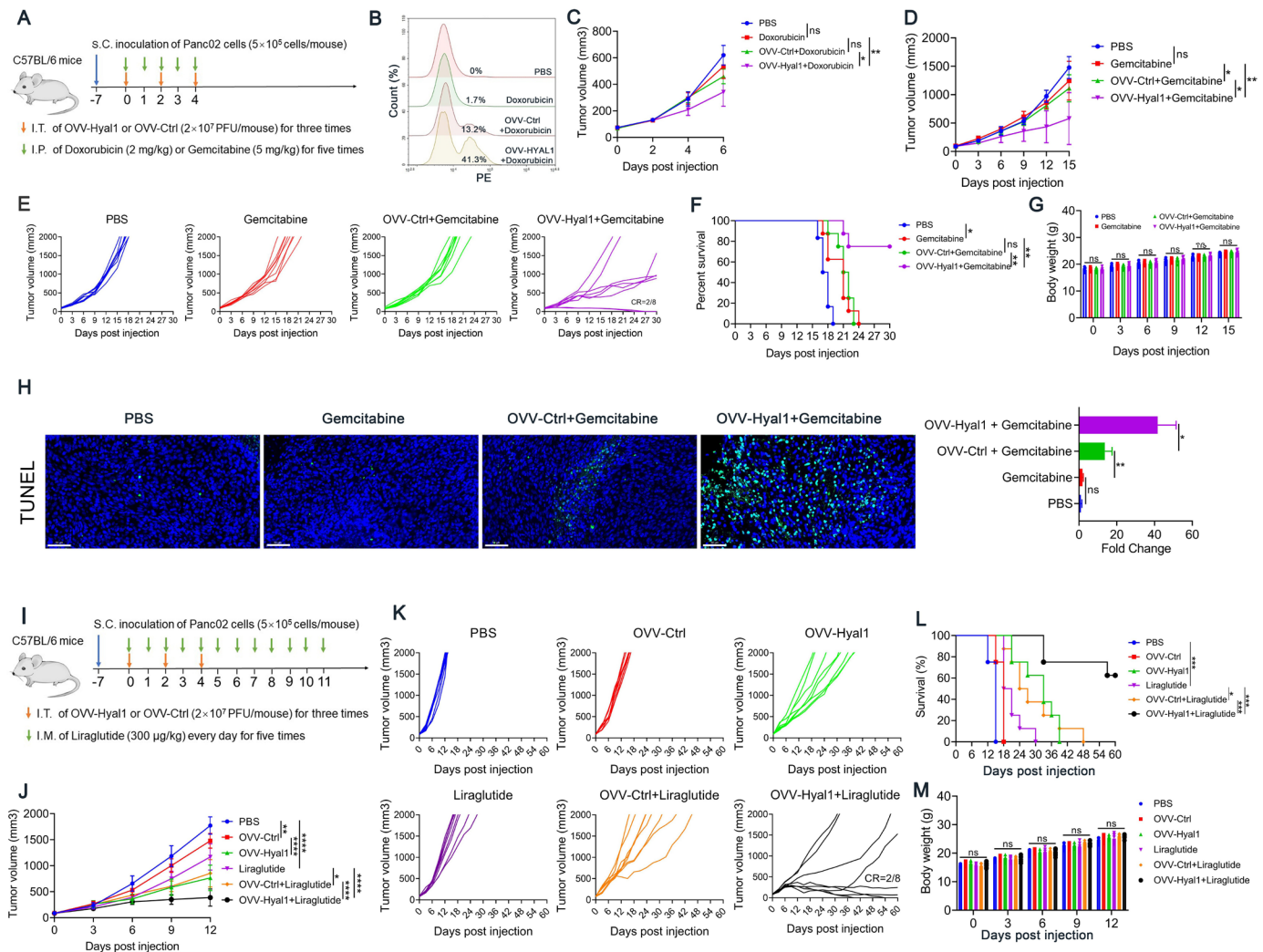
Figure 3 Oncolytic vaccinia virus encoding the hyaluronidase (OVV-Hyal1) significantly improves chemotherapy and GLP1-mediated antitumor efficacy. (A) Treatment scheme of combination OVV-Hyal1 and doxorubicin or gemcitabine in Panc02 subcutaneous tumor model. (B) Tumor single-cell suspensions were preprepared 1 day after last doxorubicin injection and analyzed by flow cytometry. Representative diagram of cell with red fluorescence in tumor tissues. (C) Mean tumor volume of combination therapy of OVV-Hyal1 and doxorubicin. (D) Mean tumor volume of combination therapy of OVV-Hyal1 and gemcitabine. (E) Individual tumor growth curve of combination therapy of OVV-Hyal1 and gemcitabine. (F) Kaplan-Meier survival curves of tumor-bearing mice. (G) Body weight of mice was measured every 3 days. (H) Induction of apoptosis in tumor tissues was assessed by terminal deoxynucleotidyl transferase dUTP nick end labeling (TUNEL) assay. Microscopic images were analyzed semi-quantitatively. Scale bars are equal to 50 μm. (I) Treatment scheme of combination OVV-Hyal1 and liraglutide in Panc02 subcutaneous tumor model. (J) Mean tumor volume of combination therapy of OVV-Hyal1 and liraglutide. (K) Individual tumor growth curve of combination therapy of OVV-Hyal1 and liraglutide. (L) Kaplan-Meier survival curves of tumor-bearing mice. (M) Body weight of mice was measured every 3 days. Error bars represent SD. ns, not significant; *p<0.05; **p<0.01; ***p<0.001; ****p<0.0001.

treatments (figure 4G). No significant changes in body weight were observed (figure 4H). To verify that OVV-Hyal1 enhances CD19 CAR-T cell infiltration in tumors, we analyzed the distribution of CD19 CAR-T cells in tumor tissue. The IHC staining revealed that OVV-Hyal1 treatment led to more CAR-T cell infiltration in tumors than both PBS and OVV-Ctrl treatment (online supplemental figure S8).

Taken together, these results indicate that ECM degradation by OVV-Hyal1 could facilitate lymphocytes infiltration and therefore improved CAR-T cells-mediated antitumor effects.

OVV-Hyal1 significantly improves the antitumor activity of CD8+ T cells and enhanced anti-PD-1-mediated antitumor efficacy in pancreatic carcinomas

Given that OVV-Hayl1 increased lymphocytes infiltration within TME, we further analyzed the antitumor activity of CD8+ T cells after OVV-Hyal1 treatment. Indeed, intratumoral injection of OVV-Hyal1 significantly increased the activation markers such as granzyme B, IFN-γ+, and CD107A in CD8+ T cells (figure 5A). Similar increase of CD8+ T activity was also observed in 4T1 breast cancer (online supplemental figure S9). Consistently, the immune activation of CD8+ T cells by OVV-Hyal1 resulted
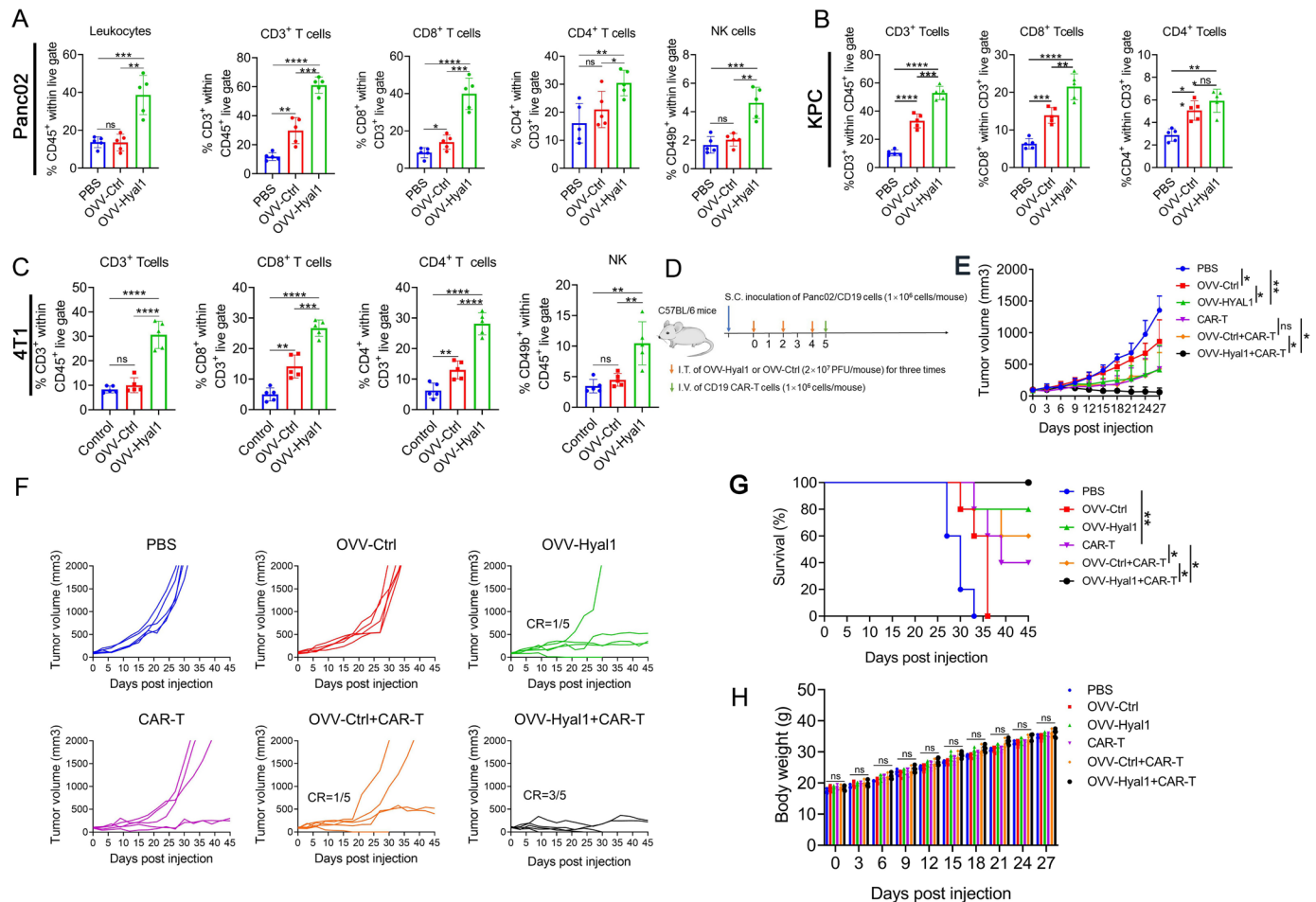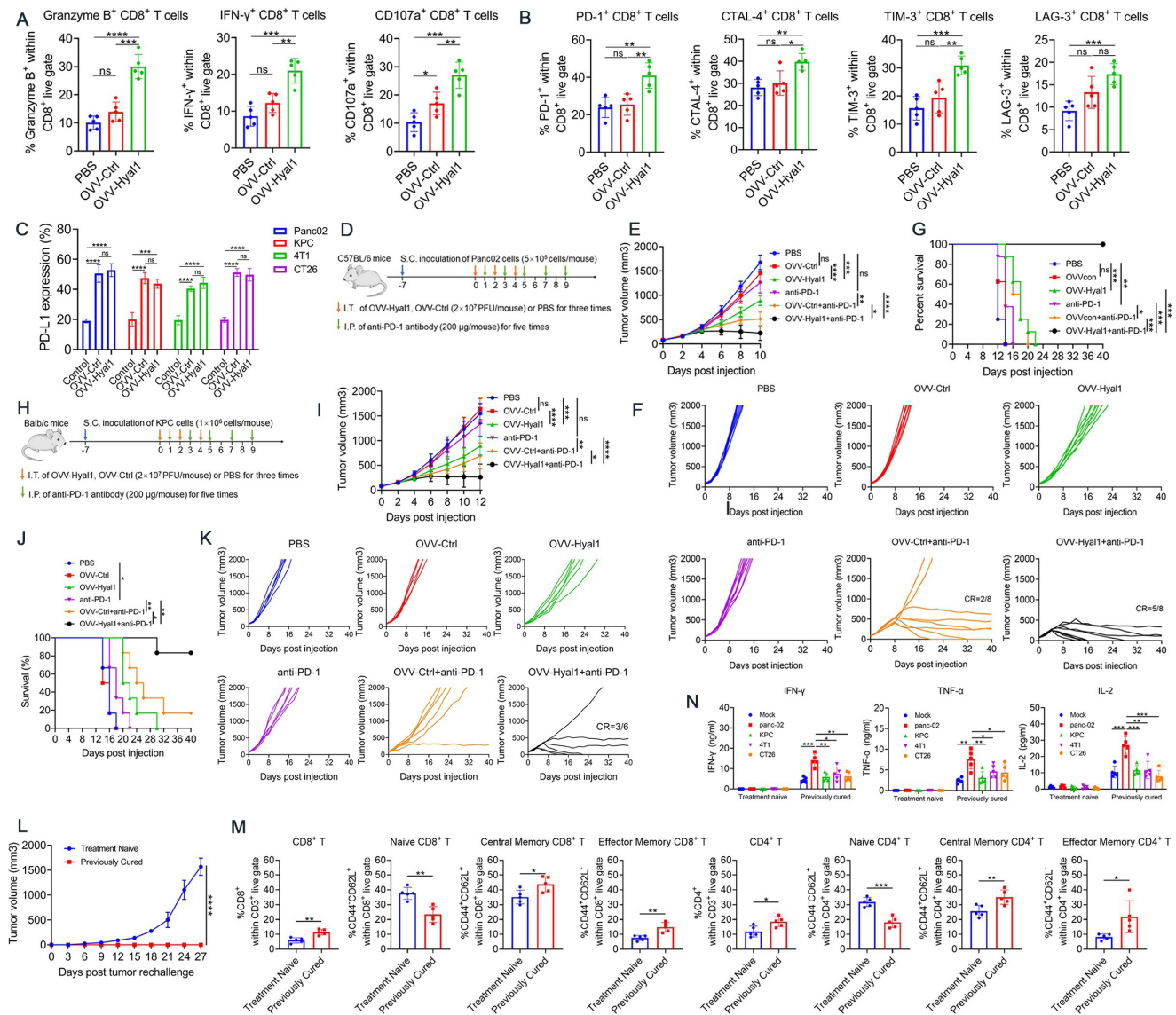
Figure 4 Oncolytic vaccinia virus encoding the hyaluronidase (OVV-Hyal1) enhances infiltration of immune cells in tumor microenvironment (TME) and sensitizes pancreatic cancer to CAR-T cell therapy. (A–C) Panc02, KPC and 4T1 models were established as described in figure 1E and the single-cell suspensions were preprepared two days after last viral injection. (A) Flow cytometric analysis of the proportion of lymphocytes, CD3⁺ T cells, CD8⁺ T cells, CD4⁺ T cells, and NK cells in Panc02 tumor tissues. (B) Flow cytometric analysis of the proportions of CD3⁺ T cells, CD8⁺ T cells, CD4⁺ T cells in KPC tumors. (C) Flow cytometric analysis of the proportion of CD8⁺ T cells, CD4⁺ T cells and NK cells in 4T1 tumor tissues. (D) Treatment scheme of combination OVV-Hyal1 and CD19 CAR-T cells in Panc02/CD19 subcutaneous tumor model. (E) Mean tumor volume of combination therapy of OVV-Hyal1 and CD19 CAR-T cells. (F) Individual tumor growth curve of combination therapy of OVV-Hyal1 and CD19 CAR-T cells. (G) Kaplan-Meier survival curves of tumor-bearing mice. (H) Body weight of mice was measured every three days. Error bars represent SD. ns, not significant; *p<0.05; **p<0.01; ***p<0.001; ****p<0.0001.

in the elevated expression of immune checkpoints including PD-1, CTLA-4, TIM-3, LAG-3 on CD8⁺ T cells (figure 5B).

In line with the above findings, transcriptomic analysis of pancreatic Panc02 tumor xenografts showed that the expression levels of immune-related genes, including Ccl2, Tnf, CD86, Myd88, Cxcl12, etc, were increased in OVV-Hyal1-injected tumors (online supplemental figure S10A). Gene ontology analysis further confirmed several enriched signalings such as T cell activation, activation of immune response, adaptive immune response, type I interferon receptor activity (online supplemental figure S10B).

Interestingly, we found that the expression of PD-L1 was significantly upregulated on Panc02, KPC, 4T1, and CT26 cell lines by either OVV-Hyal1 or OVV-Ctrl (figure 5C). We postulated that OVV-Hyal1 might improve the therapeutic

outcomes of immune checkpoint inhibitors such as PD-1 antibodies. In a pancreatic Panc02 carcinoma subcutaneous tumor model (figure 5D), OVV-Hyal1 robustly enhanced the antitumor efficacy of αPD-1 compared with each single therapy or αPD-1 in combination with OVV-Ctrl (figure 5E,F), which resulted in over 60% (five out of eight mice) complete response (figure 5F), and the significantly prolonged survival (figure 5G). No significant changes in body weight were observed (online supplemental figure S11A). Similarly, in another pancreatic KPC carcinoma model (figure 5H), OVV-Hyal1 significantly enhanced the therapeutic outcomes of αPD-1 compared with each single therapy or αPD-1 in combination with OVV-Ctrl (figure 5I,J). About 50% CRs were achieved by the combination of OVV-Hyal1 with αPD-1 (figure 5K). No significant changes in body weight were observed (online supplemental figure S11B).

Figure 5 Oncolytic vaccinia virus encoding the hyaluronidase (OVV-Hyal1) augments CD8^{+} T cells responses and sensitizes pancreatic cancer to anti-PD-1 therapy. (A, B) Panc02 were established as described in figure 1E and the single-cell suspensions were preprepared two days after last viral injection. (A) Flow cytometric analysis of the expression of granzyme B, IFN-γ and CD107A on CD8^{+} T cells in Panc02 tumor tissues. (B) Flow cytometric analysis of the expression of immune checkpoints PD-1, CTLA-4, TIM-3, and LAG-3 on CD8^{+} T cells. (C) After a 24 hours incubation of OVVs at an MOI of 0.5, tumor cells were harvested and the expression of PD-L1 and CD47 on these cells was detected by flow cytometry using anti-PD-L1 antibody or anti-CD47 antibody. Data are presented as means±SD. (D–G) Combined therapy of OVV-Hyal1 and anti-PD-1 antibody in Panc02 subcutaneous tumor model. (D) Treatment scheme of combination OVV-Hyal1 and anti-PD-1 antibody. (E) Mean tumor volume of combination therapy of OVV-Hyal1 and anti-PD-1 antibody. (F) Individual tumor growth curve of combination therapy of OVV-Hyal1 and anti-PD-1 antibody. (G) Kaplan-Meier survival curves of tumor-bearing mice. (H–K) Combined therapy of OVV-Hyal1 and anti-PD-1 antibody in KPC subcutaneous tumor model. (H) Treatment scheme of combination OVV-Hyal1 and anti-PD-1 antibody. (I) Mean tumor volume of combination therapy of OVV-Hyal1 and anti-PD-1 antibody. (J) Individual tumor growth curve of combination therapy of OVV-Hyal1 and anti-PD-1 antibody. (K) Kaplan-Meier survival curves of tumor-bearing mice. (L–N) Treatment of mice with combination OVV-Hyal1 and anti-PD-1 antibody established long-term tumor-specific immunological memory in Panc02 subcutaneous tumor model. (L–N) Combined treatment of OVV-Hyal1 and anti-PD-1 established long-term tumor-specific immunological memory. (L) The cured mice previously challenged with Panc02 and naïve mice were subcutaneously injected with Panc02 cells, and tumor volumes were measured. (M) By the end of the rechallenging experiment, spleens were obtained from either previously cured mice or naïve mice, single cell suspensions were stained and subjected to flow cytometry to detect the proportion of CD8^{+} T cells and CD4^{+} T cells, naïve (CD62L^{+}CD44^{−}), central memory (CD62L^{+}CD44^{+}) and effector memory (CD62L^{−}CD44^{+}) CD8^{+} T cells and CD4^{+} T cells. Data are presented as means±SD. (N) Splenocytes from either previously cured mice or naïve mice were co-cultured with Panc02 cells or other mouse cancer cell lines as depicted. 72 hours later, the supernatants were harvested and the cytokines including interferon-gamma (IFN-γ), tumor necrosis factor-alpha (TNF-α) and interleukin 2 (IL-2) were detected by ELISA. Data are presented as means±SD. ns, not significant; *p<0.05; **p<0.01; ***p<0.001; ****p<0.0001.

Finally, we examined the tumor-specific immunological memory, five cured mice (figure 5F) were subcutaneously rechallenged with the same pancreatic Panc02 carcinoma cell line. We found that all the previously cured mice were rejective to tumor growth, whereas all age-matched treatment-naïve mice developed xenograft tumors (figure 5L). Consistently, the proportion of spleen CD8$^+$ and CD4$^+$ T cells, as well as the respective central memory (CD62L$^+$ CD44$^+$) and effector memory (CD62L$^-$ CD44$^+$) subset T cells were increased in cured mice, whereas naïve CD8$^+$ and CD4$^+$ T cells (CD62L$^+$CD44$^-$) were significantly decreased compared with those treatment-naïve mice (figure 5M). Furthermore, the splenocytes isolated from the Panc02 rechallenged mice were co-cultured with Panc02, KPC, 4T1, and CT26 cells, respectively, and merely the splenocytes stimulated by Panc02 cells produced significantly higher levels of IFN-γ, TNF-α, and IL-2 than those stimulated by either KPC cells, 4T1 cells or CT26 cells, the splenocytes from treatment-naive mice showed undetectable cytokines to each cell line (figure 5N).

Taken together, these data indicate that OVV-Hyal1 combined with anti-PD-1 significantly improved the therapeutic outcomes in pancreatic carcinomas and could establish a long-term tumor-specific immune surveillance.

OVV-Hyal1 reshapes macrophages infiltration, polarization and improves the antitumor efficacy of αCD47

Having shown that OVV-Hyal1 increased lymphocytes infiltration, we further investigated the impacts of OVV-Hyal1 on other leukocytes such as macrophages and dendritic cells (DCs), which present phagocytosis, antigen presentation that contribute to T cell activation. OVV-Hyal1 significantly increased the infiltration of macrophages in pancreatic carcinoma as evidenced by flow cytometry (figure 6A) and by CD68$^+$ immunohistochemistry (figure 6B). Moreover, OVV-Hyal1 reshaped macrophage polarization from M2 to M1 (figure 6C). Similarly, in a 4T1 breast cancer model, OVV-Hyal1 also significantly increased the infiltration of macrophages (figure 6D). Similarly, OVV-Hyal1 significantly increased the infiltration of DCs and their activity in pancreatic carcinoma as evidenced by upregulation of CD80 and CD86 on DCs (online supplemental figure S12A). Interestingly, the number of CD11b$^+$Gr1$^+$ myeloid derived suppressor cells (MDSCs) were reduced in OVV-Hyal1-treated tumors (online supplemental figure S12B).

Since CD47 antibody has been shown to enhance the phagocytosis of macrophages by blocking the "don't eat me" signaling. We then evaluated the antitumor efficacy of OVV-Hyal1 in combination with αCD47 in an orthotopic breast cancer 4T1 model (figure 6E). Intratumoral injection of OVV-Hyal1 significantly enhanced the antitumor efficacy of αCD47 compared with each monotherapy or αCD47 in combination with OVV-Ctrl (figure 6F,G), about 50% CRs (four out of eight) were achieved (figure 6G). Consistently, OVV-Hyal1 combined with αCD47 significantly prolonged the survival time

compared with other treatments (figure 6H). No significant changes in body weight were observed (figure 6I).

Taken together, these results indicate that OVV-Hyal1 facilitated macrophage infiltration, reshaped macrophage polarization, and significantly improved the antitumor efficacy of αCD47 therapy.

DISCUSSION

Plenty of ECM in the TME limits the antitumor therapy. In this study, we showed that the novel Hyal1-armed recombinant vaccinia virus, OVV-Hyal1, reshaped the TME by degradation of HA and consequently facilitated intratumoral virus spread, chemo drugs diffusion, leukocytes infiltration, and immune activation. In several solid tumor models, OVV-Hyal1 significantly enhanced the antitumor outcomes of chemo drugs such as doxorubicin and gemcitabine, polypeptide liraglutide, checkpoint inhibitors PD-1 and CD47 antibodies, and CAR-T cells. Our work provides an effective solution to overcome the hurdles of tumor ECM in cancer therapy.

Intratumoral spread of OVs is associated with the antitumor efficacy. ECM has been shown to limit the viral vector spread, and degradation of ECM with proteolytic enzymes such as relaxin or collagenase enhanced viral propagation in the tumor bulk and improved viral vector distribution following intratumoral delivery.[25–27] Adenovirus expressing hyaluronidase or intravenous coadministration of hyaluronidase and oncolytic adenovirus could boost viral dispersion and improve therapeutic efficacy in vivo.[18 28 29] In line with these findings, the enhanced antitumor effects of OVV-Hyal1 compared with OVV-Ctrl in different tumor models was attributed to two aspects: (i) the facilitated virus spread of OVV-Hyal1 by degradation of ECM; (ii) the increased antitumor immune activity of the infiltrating CD8$^+$ T cells.

Accumulation of excessive HA could lead to the increase of interstitial pressure, which together with ECM established a physical barrier to chemo drugs.[30] The excessive ECM also induced anoikis resistance and cell adhesion-mediated drug resistance.[31 32] In several preclinical studies, PEG-PH20, a pegylated recombinant human hyaluronidase, has been proven to degrade HA and remodel tumor stroma, thus improved perfusion and drug delivery.[33] A recent phase II clinical trial showed that PEG-PH20 combined with gemcitabine and Nab-paclitaxel improved progression-free survival in metastatic pancreatic ductal adenocarcinoma (PDAC) patients treated.[15] Unfortunately, the phase III trial showed that the overall survival was not improved by addition of PEG-PH20 to gemcitabine and Nab-paclitaxel, therefore did not support further development of PEG-PH20 in metastatic PDAC.[34] The off-target effect of PEG-PH20 system administration might be the reason for its unsatisfactory clinical outcomes. Nevertheless, our work provides an alteration by combining OVV-Hyal1 with chemo drugs. Intratumoral administration of OVV-Hyal1 and consequently local expression of hyaluronidase led to a more
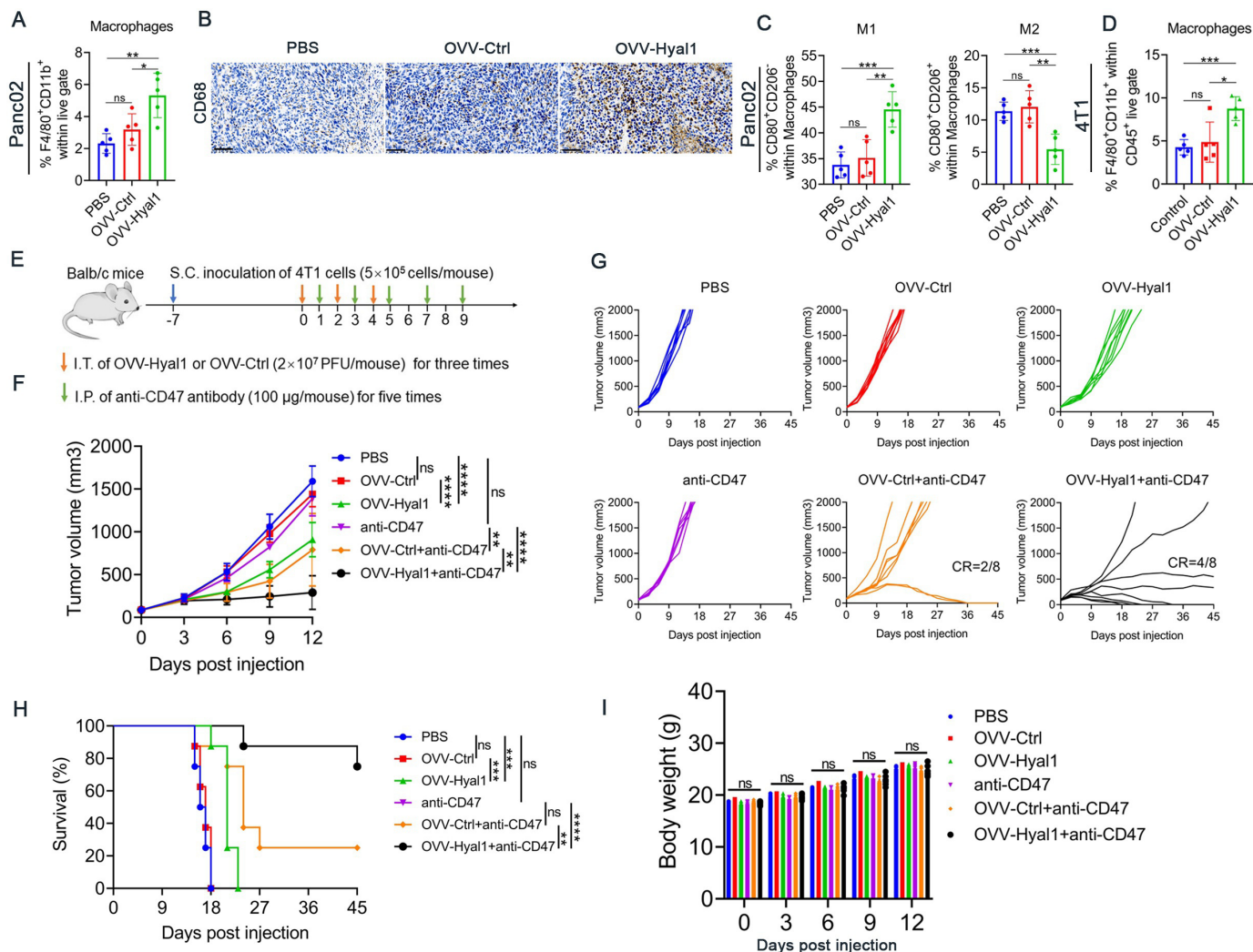
Figure 6 Oncolytic vaccinia virus encoding the hyaluronidase (OVV-Hyal1) promotes macrophages infiltration and M1 polarization and sensitizes breast cancer to anti-CD47 therapy. (A, C, D) Panc02 and 4T1 tumor models were established as described in figure 1E and the single-cell suspensions were preprepared two days post the last viral injection. (A) Flow cytometric analysis of the proportions of F4/80$^+$CD11b$^+$ macrophages in Panc02 model. Data are presented as means±SD. (B) Immunohistochemistry for CD68 in Panc02 model. The establishment of the Panc02 model and the treatment scheme was similar to figure 1E. Immunohistochemical staining was used to detect the infiltration of CD68$^+$ T cells in the tumor tissue of the Panc02 subcutaneous model. Scale bar represents 50 μm. (C) Flow cytometric analysis of the proportions of CD80$^+$CD206$^-$ M1 macrophages and CD80$^+$CD206$^+$ M2 macrophages in Panc02 model. Data are presented as means±SD. (D) Flow cytometric analysis of the proportions of F4/80$^+$CD11b$^+$ macrophages in 4T1 model. Data are presented as means±SD. (E) Treatment scheme of combination OVV-Hyal1 and anti-CD47 antibody in 4T1 subcutaneous tumor model. (F) Mean tumor volume of combination therapy of OVV-Hyal1 and anti-CD47 antibody. (G) Individual tumor growth curve of combination therapy of OVV-Hyal1 and anti-CD47 antibody. (H) Kaplan-Meier survival curves of tumor-bearing mice. (I) Body weight of mice was measured every three days. Error bars represent SD. ns, not significant; *p<0.05; ***p<0.001; ****p<0.0001.

effective HA degradation, which improved diffusion of chemo drugs as well as chemo drug-induced apoptosis. In parallel, local expression of HA minimized its systemic off-target side effects.

Interestingly, OVV-Hyal1 not only improved the therapeutic outcomes of the chemo drugs, but also significantly enhanced the antitumor efficacy of a polypeptide liraglutide, which has been shown to enhance antitumor immune responses.[24] This opens a door for combining ECM degradation with polypeptide drugs to enhance therapeutic outcomes.

Stiff ECM not only acts as a physical barrier to chemo drugs, but also limits the leukocytes penetration into malignancies and handicaps the antitumor immune responses. For instance, in both PDAC and lung cancer, ECM density and architecture sequestered T cell in tumor stroma and limited their infiltration to tumor nests.[35–37] In contrast, loose fibronectin and collagen regions facilitated T cell migration.[36] In line, local HA degradation by OVV-Hyal1 significantly increased leukocytes infiltration, and further increased the antitumor immune activity of CD8$^+$ T cells, which was probably attributed to the increase

of TME-infiltrating DCs and their activity, as well as to the reduced MDSCs within TME by OVV-Hyal1 as shown in our study. However, it remains to be further clarified how OVV-Hyal1-mediated HA degradation increased the activity of DCs.

The HA degradation and ECM remodeling by OVV-Hyal1 may also provide a shortcut for CAR-T cell-based therapy in solid tumors. Since CAR-T encountered the similar physical ECM hurdles as other autonomous lymphocytes.[12] On the one hand, local injection of OVV-Hyal1 could attracted CAR-T cells to the tumor region, on the other hand, OVV-Hyal1 eased infiltration/migration of CAR-T cells to tumor nests to exert their tumor specific cytotoxicity. Therefore, OVV-Hyal1 represents a potential candidate to overcome the current setbacks of CAR T-cell application in pancreatic cancer therapy.

In addition to improvement of chemotherapy and CAR-T cell-based therapy, OVV-Hyal1 also significantly enhanced the antitumor effects of ICBs in several solid tumors. This makes the OVV-Hyal1 attractive for cancer immunotherapy. Intratumoral administration of OVV-Hyal1 not only recruited immune cells to the tumor region, but also facilitated their infiltration/migration in TME, when further combined with ICBs such as PD-1 or CD47 antibodies to block immune evasion, more efficient antitumor outcomes could be achieved as observed in the current study.

Theoretically, tumor invasion and metastasis are related to factors such as cytoskeleton and tumor angiogenesis, both are regulated by ECM.[38] As an important component of ECM, HA can affect the above processes by interacting with receptors. Previous study showed that interaction between HA and CD44 affected tumor growth, metastasis, and tumor angiogenesis. However, in a metastatic breast cancer model, we did not see any increase of remote metastases on OVV-Hyal1 treatment. Nevertheless, other metastatic models should be further investigated before OVV-Hyal1 can be translated into clinical trials.

In summary, OVV-Hyal1-mediated HA degradation in solid tumors reshaped TME, which facilitated viral spread, chemo drug diffusion and leukocytes infiltration in TME, these features of OVV-Hyal1 significantly improved the antitumor outcomes of chemotherapy, polypeptide-mediated therapy, CAR-T cell-based therapy, and ICBs. It merits further exploration of OVV-Hyal1 for clinical trials for solid malignancies. Particularly, given that currently available therapies for advanced PDAC are modestly effective, the clinical effectiveness of OVV-Hyal1 might be best evaluated in patients with advanced PDAC in combination with gemcitabine or ICBs.

Competing interests No, there are no competing interests.

Patient consent for publication Not applicable.

Ethics approval All animal procedures and experiments were performed following the guidelines that had been approved by the Animal Care and Use Committee of Nanjing University (D2202123).

Provenance and peer review Not commissioned; externally peer reviewed.

Data availability statement Data are available upon reasonable request.

Supplemental material This content has been supplied by the author(s). It has not been vetted by BMJ Publishing Group Limited (BMJ) and may not have been peer-reviewed. Any opinions or recommendations discussed are solely those of the author(s) and are not endorsed by BMJ. BMJ disclaims all liability and responsibility arising from any reliance placed on the content. Where the content includes any translated material, BMJ does not warrant the accuracy and reliability of the translations (including but not limited to local regulations, clinical guidelines, terminology, drug names and drug dosages), and is not responsible for any error and/or omissions arising from translation and adaptation or otherwise.

ORCID iD
Jiwu Wei http://orcid.org/0000-0002-0883-1824

REFERENCES

1. Cox TR. The matrix in cancer. *Nat Rev Cancer* 2021;21:217–38.
2. Chanmee T, Ontong P, Itano N. Hyaluronan: A modulator of the tumor Microenvironment. *Cancer Lett* 2016;375:20–30.
3. Whatcott CJ, Han H, Posner RG, *et al.* Targeting the tumor Microenvironment in cancer: why Hyaluronidase deserves a second look. *Cancer Discov* 2011;1:291–6.
4. Toole BP. Hyaluronan: from extracellular glue to Pericellular cue. *Nat Rev Cancer* 2004;4:528–39.
5. Whatcott CJ, Han H, Von Hoff DD. Orchestrating the tumor Microenvironment to improve survival for patients with Pancreatic cancer: normalization, not destruction. *Cancer J* 2015;21:299–306.
6. Ropponen K, Tammi M, Parkkinen J, *et al.* Tumor cell-associated Hyaluronan as an unfavorable Prognostic factor in colorectal cancer. *Cancer Res* 1998;58:342–7.
7. Setälä LP, Tammi MI, Tammi RH, *et al.* Hyaluronan expression in gastric cancer cells is associated with local and nodal spread and reduced survival rate. *Br J Cancer* 1999;79:1133–8.
8. Auvinen P, Tammi R, Parkkinen J, *et al.* Hyaluronan in peritumoral Stroma and malignant cells Associates with breast cancer spreading and predicts survival. *Am J Pathol* 2000;156:529–36.
9. Lipponen P, Aaltomaa S, Tammi R, *et al.* High Stromal Hyaluronan level is associated with poor differentiation and metastasis in prostate cancer. *Eur J Cancer* 2001;37:849–56.
10. Anttila MA, Tammi RH, Tammi MI, *et al.* High levels of Stromal Hyaluronan predict poor disease outcome in epithelial ovarian cancer. *Cancer Res* 2000;60:150–5.
11. Ishihara J, Ishihara A, Sasaki K, *et al.* Targeted antibody and cytokine cancer Immunotherapies through collagen affinity. *Sci Transl Med* 2019;11:487.
12. Rezaei R, Esmaeili Gouvarchin Ghaleh H, Farzanehpour M, *et al.* Combination therapy with CAR T cells and Oncolytic viruses: a new era in cancer Immunotherapy. *Cancer Gene Ther* 2022;29:647–60.
13. He J, Baum LG. Presentation of Galectin-1 by extracellular matrix triggers T cell death. *J Biol Chem* 2004;279:4705–12.
14. Clift R, Souratha J, Garrovillo SA, *et al.* Remodeling the tumor Microenvironment sensitizes breast tumors to anti-programmed death-ligand 1 Immunotherapy. *Cancer Res* 2019;79:4149–59.
15. Hingorani SR, Zheng L, Bullock AJ, *et al.* HALO 202: randomized phase II study of Pegph20 plus NAB-paclitaxel/Gemcitabine versus NAB-paclitaxel/Gemcitabine in patients with untreated, metastatic Pancreatic Ductal adenocarcinoma. *JCO* 2018;36:359–66.
16. Guan X, Chen J, Hu Y, *et al.* Highly enhanced cancer Immunotherapy by combining Nanovaccine with Hyaluronidase. *Biomaterials* 2018;171:198–206.
17. Jang SH, Wientjes MG, Lu D, *et al.* Drug delivery and transport to solid tumors. *Pharm Res* 2003;20:1337–50.

18 Guedan S, Rojas JJ, Gros A, *et al*. Alemany R: Hyaluronidase expression by an Oncolytic adenovirus enhances its Intratumoral spread and suppresses tumor growth. *Mol Ther* 2010;18:1275–83.

19 Wang S, Yan W, Kong L, *et al*. Oncolytic viruses engineered to enforce cholesterol efflux restore tumor-associated macrophage Phagocytosis and anti-tumor immunity in glioblastoma. *Nat Commun* 2023;14.

20 Shalhout SZ, Miller DM, Emerick KS, *et al*. Therapy with Oncolytic viruses: progress and challenges. *Nat Rev Clin Oncol* 2023;20:160–77.

21 Zuo S, Wei M, Xu T, *et al*. An engineered Oncolytic Vaccinia virus Encoding a single-chain variable fragment against TIGIT induces effective antitumor immunity and Synergizes with PD-1 or LAG-3 blockade. *J Immunother Cancer* 2021;9:12.

22 Stromnes IM, Schmitt TM, Hulbert A, *et al*. T cells engineered against a native antigen can surmount immunologic and physical barriers to treat Pancreatic Ductal adenocarcinoma. *Cancer Cell* 2015;28:638–52.

23 Jiang H, Hegde S, Knolhoff BL, *et al*. Targeting focal adhesion kinase renders Pancreatic cancers responsive to Checkpoint Immunotherapy. *Nat Med* 2016;22:851–60.

24 Lu X, Xu C, Dong J, *et al*. Liraglutide activates nature killer cell-mediated antitumor responses by inhibiting IL-6/Stat3 signaling in hepatocellular carcinoma. *Transl Oncol* 2021;14.

25 Kuriyama N, Kuriyama H, Julin CM, *et al*. Protease pretreatment increases the efficacy of adenovirus-mediated gene therapy for the treatment of an experimental glioblastoma model. *Cancer Res* 2001;61:1805–9.

26 Lee WJ, Ahn HM, Roh H, *et al*. Decorin-expressing adenovirus decreases collagen synthesis and Upregulates MMP expression in Keloid fibroblasts and Keloid Spheroids. *Exp Dermatol* 2015;24:591–7.

27 Jung KH, Choi I-K, Lee H-S, *et al*. Oncolytic adenovirus expressing Relaxin (Ydc002) enhances therapeutic efficacy of Gemcitabine against Pancreatic cancer. *Cancer Lett* 2017;396:155–66.

28 Farrera-Sal M, Moreno R, Mato-Berciano A, *et al*. Alemany R: Hyaluronidase expression within tumors increases Virotherapy efficacy and T cell accumulation. *Mol Ther Oncolytics* 2021;22:27–35.

29 Ganesh S, Gonzalez-Edick M, Gibbons D, *et al*. Intratumoral coadministration of Hyaluronidase enzyme and Oncolytic Adenoviruses enhances virus potency in metastatic tumor models. *Clin Cancer Res* 2008;14:3933–41.

30 Jacobetz MA, Chan DS, Neesse A, *et al*. Hyaluronan impairs vascular function and drug delivery in a mouse model of Pancreatic cancer. *Gut* 2013;62:112–20.

31 Islam MS, Ciavattini A, Petraglia F, *et al*. Extracellular matrix in uterine Leiomyoma pathogenesis: a potential target for future Therapeutics. *Hum Reprod Update* 2018;24:59–85.

32 Wang L, Li C, Wang J, *et al*. Transformable ECM deprivation system effectively suppresses renal cell carcinoma by reversing Anoikis resistance and increasing chemotherapy sensitivity. *Advanced Materials* 2022;34:43. 10.1002/adma.202203518 Available: https://onlinelibrary.wiley.com/toc/15214095/34/43

33 Morosi L, Meroni M, Ubezio P, *et al*. Kang DW et al: pegylated recombinant human Hyaluronidase (Pegph20) pre-treatment improves intra-tumour distribution and efficacy of paclitaxel in Preclinical models. *J Exp Clin Cancer Res* 2021;40:286.

34 Van Cutsem E, Tempero MA, Sigal D, *et al*. Randomized phase III trial of Pegvorhyaluronidase Alfa with NAB-paclitaxel plus Gemcitabine for patients with Hyaluronan-high metastatic Pancreatic adenocarcinoma. *J Clin Oncol* 2020;38:3185–94.

35 Salmon H, Franciszkiewicz K, Damotte D, *et al*. Matrix architecture defines the preferential localization and migration of T cells into the Stroma of human lung tumors. *J Clin Invest* 2012;122:899–910.

36 Wolf K, Te Lindert M, Krause M, *et al*. Physical limits of cell migration: control by ECM space and nuclear deformation and tuning by proteolysis and Traction force. *J Cell Biol* 2013;201:1069–84.

37 Hartmann N, Giese NA, Giese T, *et al*. Prevailing role of contact guidance in Intrastromal T-cell trapping in human Pancreatic cancer. *Clin Cancer Res* 2014;20:3422–33.

38 Sutherland TE, Dyer DP, Allen JE. The extracellular matrix and the immune system: A mutually dependent relationship. *Science* 2023;379.

Supplemental material

BMJ Publishing Group Limited (BMJ) disclaims all liability and responsibility arising from any reliance placed on this supplemental material which has been supplied by the author(s)

J Immunother Cancer

An oncolytic vaccinia virus encoding hyaluronidase reshapes the extracellular matrix to enhance cancer chemo- and immunotherapy

Graphical Abstract
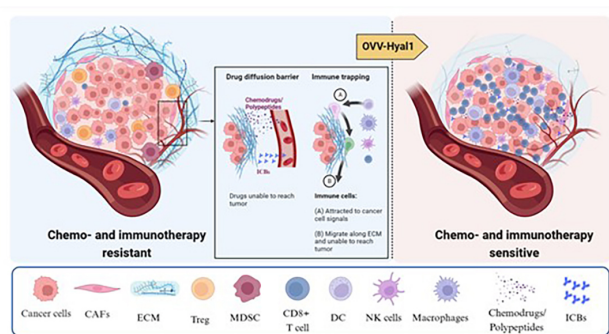
Authors

Shibing Wang, Yuxin Li, Chuning Xu, Jie Dong, Jiwu Wei

Correspondence

wjw@ nju.edu.cn (J.W.)

In Brief

The redundant ECM within solid TME often limits intratumoral diffusion of antitumor drugs, or hinders infiltration of immune cells, which results in poor antitumor efficacy of chemo- and immunotherapy. Wang et al. engineered a novel recombinant oncolytic vaccinia virus encoding the hyaluronidase (OVV-Hyal1) to reshape the ECM by degrading hyaluronic acid, a major component of ECM of many solid tumors, therefore, circumvented some major hurdles in current cancer therapy.

Highlights

- OVV-Hyal1 reshapes the ECM of solid tumors via HA degradation.

- OVV-Hyal1 facilitates virus spread, chemodrug dissemination, and immune cells infiltration within TME.

- OVV-Hyal1 significantly improves the antitumor outcomes of doxorubicin, gemcitabine, polypeptide GLP1, CAR-T cells and ICBs such as PD-1 and CD47 antibodies in a serial of solid tumors.

Supplemental material

BMJ Publishing Group Limited (BMJ) disclaims all liability and responsibility arising from any reliance placed on this supplemental material which has been supplied by the author(s)

J Immunother Cancer
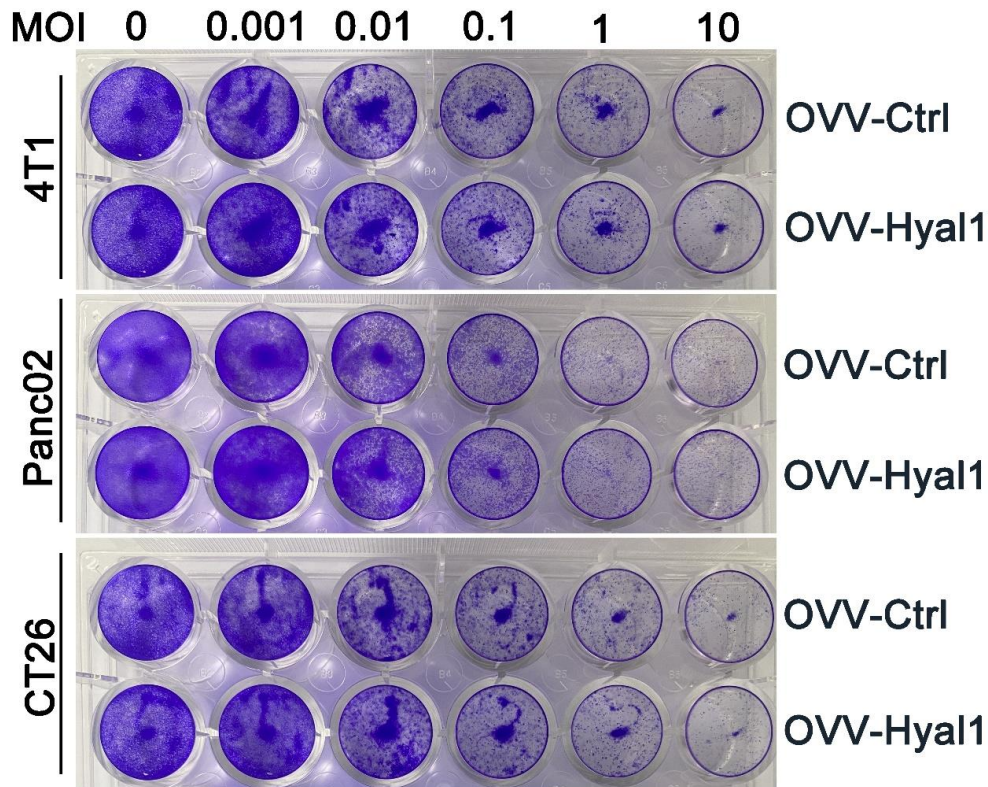
Supplementary Figures S1-12 and legends

Figure S1. Comparison of the oncolysis between OVV-Hyal1 and OVV-Ctrl. 5×10^{4} cells 4T1 breast cancer cells, Panc02 pancreatic carcinoma cells and CT26 colorectal cancer cells were seeded in 24-well plates. Then cells were treated with either OVV-Hyal1 or OVV-Ctrl at a serial of MOIs as depicted. 72 h later, cells were stained by crystal violet.
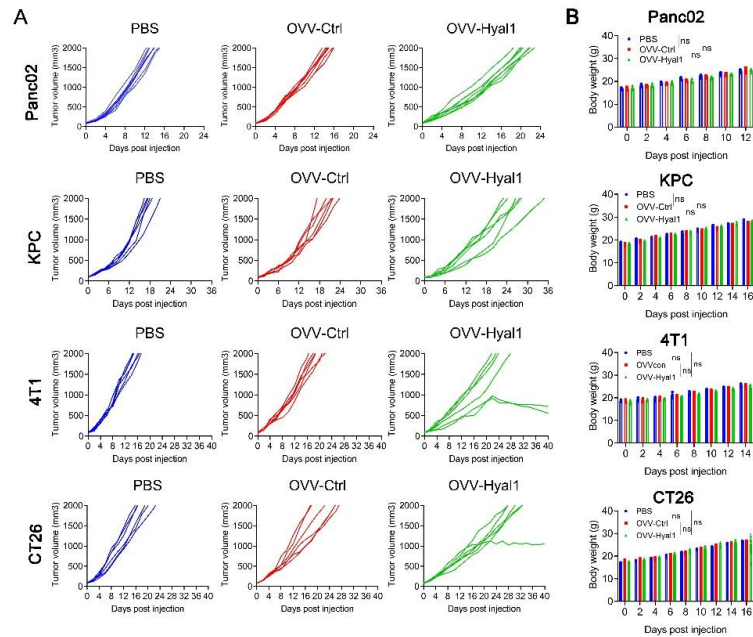
Figure S2. In vivo antitumor effects of OVV-Hyal1 and OVV-Ctrl. 5×10^5 Panc02, 1×10^6 KPC, 5×10^5 4T1 and 1×10^6 CT26 were inoculated into the right flank of C57BL/6 or BALB/c mice. When tumor volume reached approximately 50 to 100 mm^3, mice were administered intratumorally (I.T.) with either 2×10^7 pfu OVV-Hyal1 or OVV-Ctrl every other day for a total 3 times. Mice received PBS intratumoral injections were used as untreated controls. (A) The tumor volume was measured every two days until the volume exceeded 2000 mm^3. (B) Body weight of mice was measured every two days. Error bars represent SD. ns, not significant.

Supplemental material

BMJ Publishing Group Limited (BMJ) disclaims all liability and responsibility arising from any reliance placed on this supplemental material which has been supplied by the author(s)

J Immunother Cancer
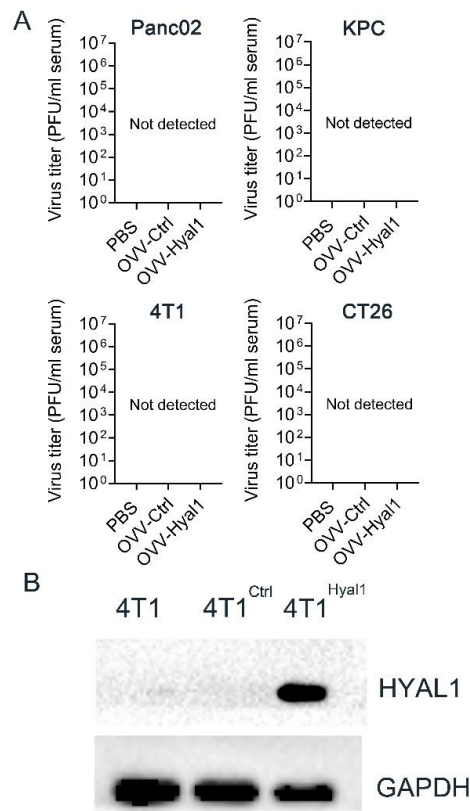
Figure S3. (A) The viral titers in the sera obtained from mice bearing Panc02, KPC, 4T1 and CT26, respectively, were quantified by TCID50 assay. (B) HYAL1 expression was determined in 4T1 cells stably expressing HYAL1 (4T1Hyal1), or parental 4T1 cells by western blot.
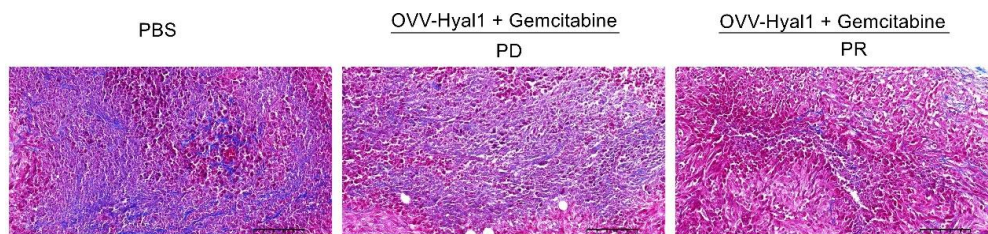

Figure S4. Differential degradation of ECM by OVV-Hyal1 in Panc02 tumors. Subcutaneous Panc02 tumors were treated with OVV-Hyal1 and gemcitabine. Then tumor tissue were obtained 30 days after the treatment from the mice with either partial remission (PR) or progressive disease (PD), respectively. Masson staining was

used to analyze the ECM degradation. Collagen was stained in blue. Scale bars are equal to 100 µm.
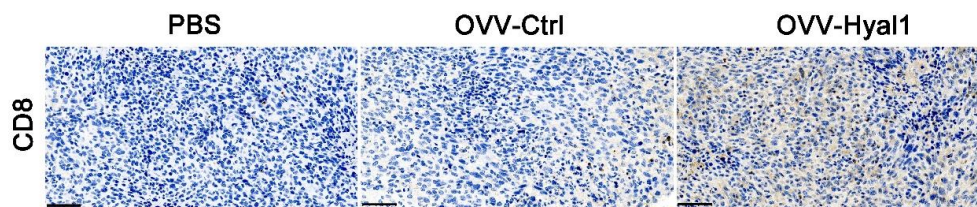

Figure S5. Immunohistochemistry for CD8 in Panc02 model. 5×10^5 Panc02 were inoculated into the right flank of C57BL/6 mice. When tumor volume reached approximately 50 to 100 mm³, mice were administered intratumorally (I.T.) with either 2×10^7 pfu OVV-Hyal1 or OVV-Ctrl every other day for a total 3 times. Mice received PBS intratumoral injections were used as untreated controls. Tumor tissue were obtained 2 days after last viral injection, and infiltration of CD8⁺ T cells in tTME was determined by immunohistochemical staining. Scale bar are equal to 50 µm.
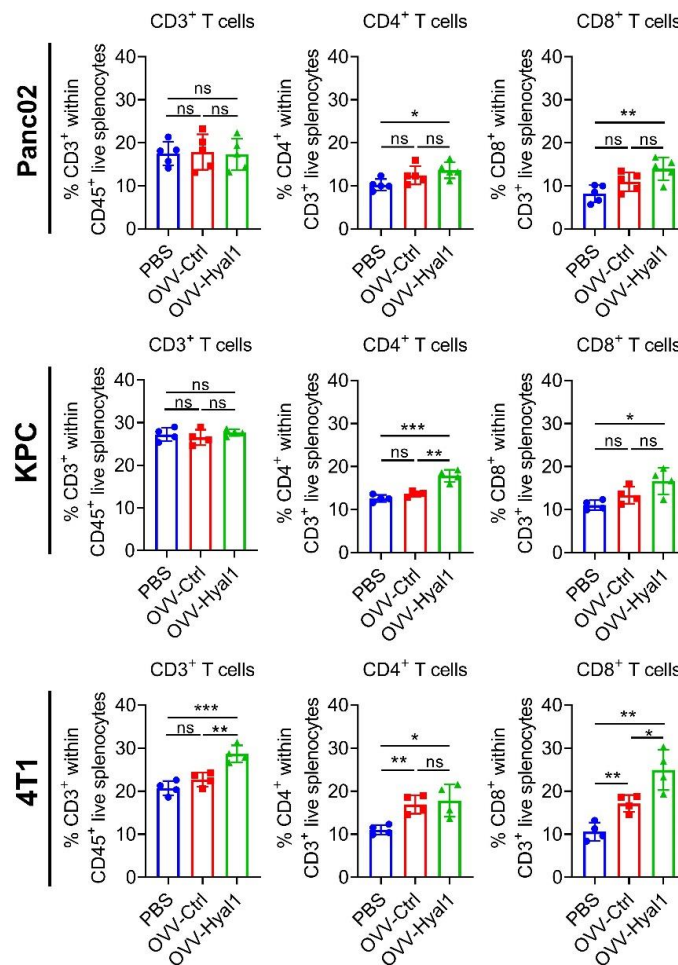
Figure S6. Flow cytometric analysis of the proportion of $CD3^+$, $CD8^+$ and $CD4^+$ T cells in splenocytes. Panc02, KPC and 4T1 models were established as previously described in Figure 1E and the single-cell suspensions were preprepared two days after last viral injection. Error bars represent SD. ns, not significant; $*p<0.05$; $**p<0.01$; $***p<0.001$.
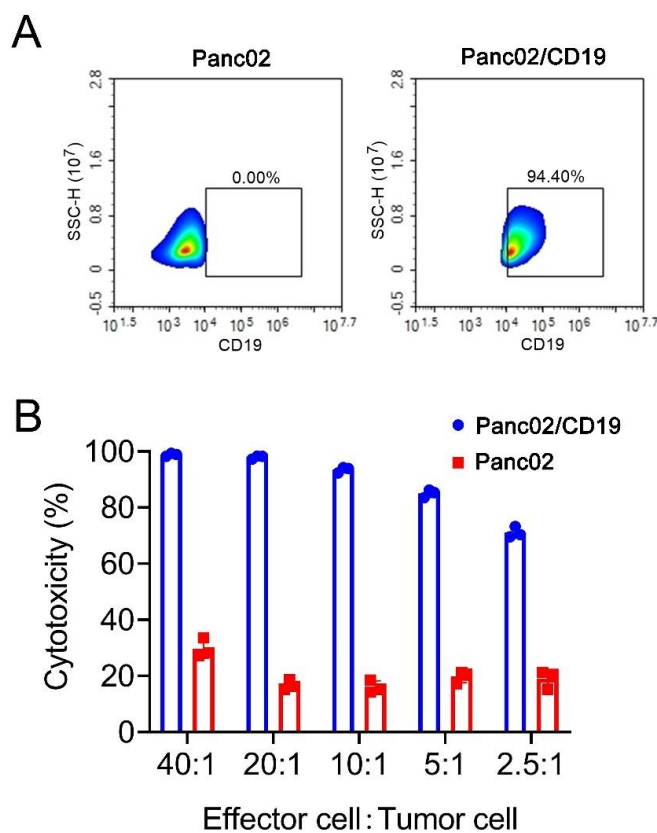
Supplemental material

BMJ Publishing Group Limited (BMJ) disclaims all liability and responsibility arising from any reliance placed on this supplemental material which has been supplied by the author(s)

J Immunother Cancer

Figure S7. Characterization of Panc02/CD19 cells. (A) Panc-02/CD19 cell line was stably expressed the human CD19 antigen, which was detected by flow cytometry. (B) Panc-02/CD19 served as the tumor target of CD19 CAR-T cells. The CD19-CAR-T cells were co-cultured with Panc02/CD19 or parental panc-02 cells with luciferase reporter gene in round bottom 96-well-plates at different ET ratios for 24 h. Error bars represent SD.

Supplemental material

BMJ Publishing Group Limited (BMJ) disclaims all liability and responsibility arising from any reliance placed on this supplemental material which has been supplied by the author(s)
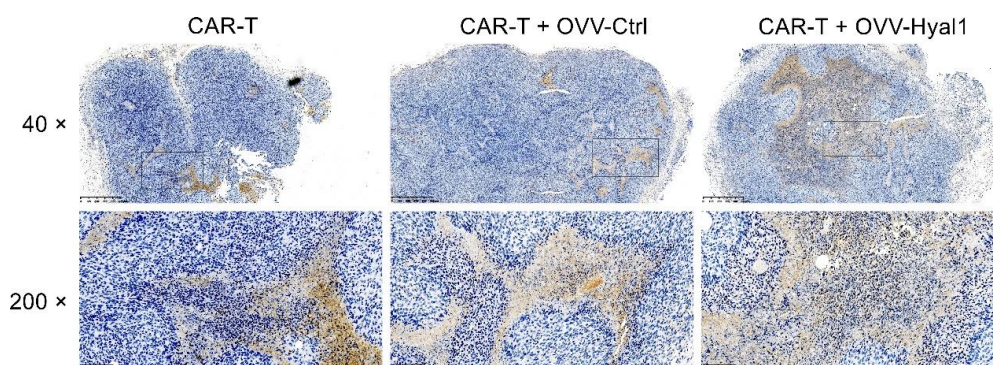
J Immunother Cancer

Figure S8. Distribution of CD19 CAR-T cells in the tumor tissue in Panc02/CD19 subcutaneous model. The establishment of the Panc02/CD19 model and the treatment scheme have been shown in Figure 4D. Immunohistochemistry in Panc02 model. Immunohistochemical staining for FMC63 scFv (brown staining) was used to detect the infiltration of CD19 CAR-T cells in the tumor tissue. Scale bars are equal to 625 µm (upper panel) and 100 µm (lower panel), respectively.
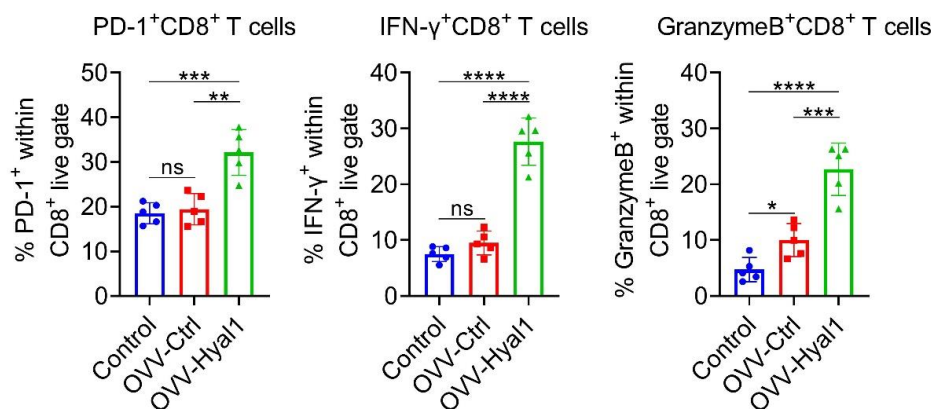

Figure S9. Immune activation status of CD8$^+$ T cells after treatment. 4T1 models were established as previously described in Figure 1E, single cell suspensions were preprepared two days after last viral injection and subjected to flow cytometry to analyze the PD-1, IFN-γ and Granzyme B expression on CD8$^+$ T cells. Error bars represent SD. ns, not significant; **$p < 0.01$; *** $p < 0.001$; **** $p < 0.0001$.
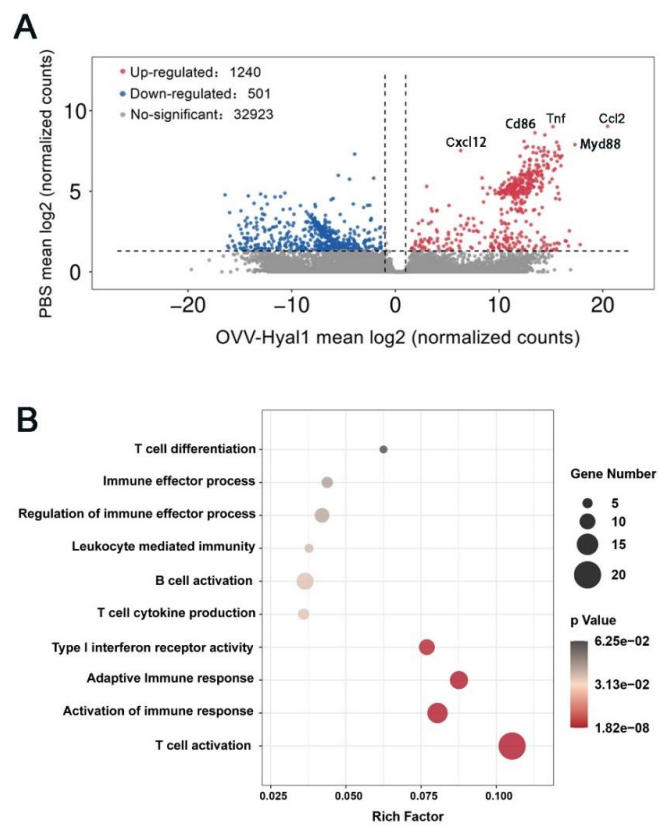
Figure S10. Gene expression in the TME by RNA-seq analysis. (A) Tumors treated with OVV-Hyal1 for 10 days were harvested, and gene expression analysis was performed using RNA-seq. The differential gene expression between the samples treated with OVV-Hyal1 and PBS, using the absolute value of logFC greater than 1 as the threshold. (B) Top 10 gene ontology enrichment terms of DEGs. Bar size indicates the number of DEGs in that gene class, and the color reflects the p value of the enriched term. The p value is higher from red to black.
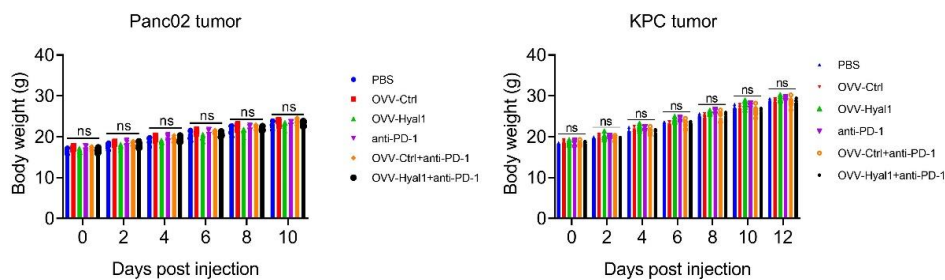
Figure S11. Body weight monitoring during therapy. Mice body weight were observed in Panc02 (A) and KPC (B) pancreatic subcutaneous tumor model treated with combined therapy of OVV-Hyal1 and anti-PD-1 antibody. Error bars represent SD. ns, not significant.
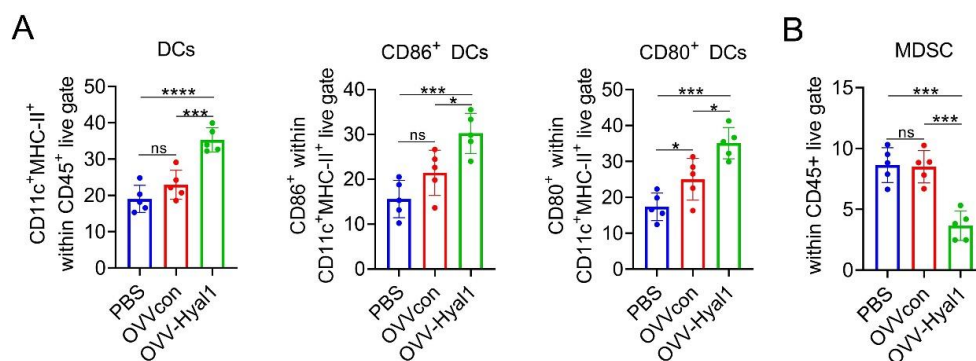

Figure S12. OVV-Hyal1 significantly increased the infiltration of DCs and their activity in pancreatic carcinoma. Panc02 models were established as previously described in Figure 1E and the single-cell suspensions were preprepared two days after last viral injection. (A) Flow cytometric analysis of the proportions of CD11c$^+$ MHC class II$^+$ dendritic cells in CD45$^+$ cells, CD86$^+$ or CD80$^+$ mature dendritic cells in CD45$^+$ CD11c$^+$ MHC class II$^+$ cells in Panc02 tumors. (B) Flow cytometric analysis of the proportions of CD11b$^+$ Gr-1$^+$ MDSC cells in CD45$^+$ cells in Panc02 tumors. Error bars represent SD. ns, not significant; * $p < 0.05$; *** $p < 0.001$; **** $p < 0.0001$.